Research Square

Preprints are preliminary reports that have not undergone peer review.
They should not be considered conclusive, used to inform clinical practice,
or referenced by the media as validated information.

Evolving initial conditions: An alternative developmental route to morphological diversity

Berta Verd

berta.verdfernandez@biology.ox.ac.uk

University of Oxford

Shannon Taylor

University of Oxford https://orcid.org/0000-0003-3490-3307

James Hammond

University of Cambridge https://orcid.org/0000-0001-9603-3410

Article

Keywords:

Posted Date: November 5th, 2026

DOI: https://doi.org/10.21203/rs.3.rs-11321337/v1

License: This work is licensed under a Creative Commons Attribution 4.0 International License.
Read Full License

Additional Declarations: There is **NO** Competing Interest.

Evolving initial conditions: An alternative developmental route to morphological diversity

Shannon E. Taylor [1], **James E. Hammond** [1], **Berta Verd** [1*]
[1]Department of Biology, University of Oxford, United Kingdom
[*]Correspondence: berta.verdfernandez@biology.ox.ac.uk

ABSTRACT

Phenotypic diversity is often thought to arise from the evolutionary modification of developmental processes. However, developmental processes are tightly coupled in space and time, with each process initiating from conditions set by prior developmental processes. While dynamical systems theory predicts that such initial conditions majorly determine a system's outcome, their importance as a source of phenotypic evolvability has been largely overlooked. Here we we provide empirical evidence that phenotypic evolution can proceed through changes in developmental initial conditions while the underlying developmental process remains conserved. Somitogenesis is the process by which vertebral precursors, known as somites, are periodically formed from the pre-somitic mesoderm (PSM). Somite count (the total number of somites formed during development which will ultimately determine vertebral counts) is thought to diversify through the evolution of components of somitogenesis such as the frequency of the segmentation clock or the mechanisms driving axial morphogenesis. In studying two closely related species of Lake Malawi cichlid fishes that differ in their total number of vertebrae, we show that somite count has evolved without changes to somitogenesis itself, rather by altering the size of the PSM at the onset of this process. This work expands what we consider developmental drivers of phenotypic evolution and highlights the importance of comparative studies in understanding the evolutionary diversification of phenotypes.

INTRODUCTION

One of the longest-standing questions in biology is how organisms evolve to generate the remarkable diversity of forms that we see in the natural world (Darwin, 1859). This 'evolvability' underlies life's ability to adapt to ever-changing environments and exploit new eco-

logical opportunities, resulting in a spectacular range of morphologies and innovations across the tree of life. The evolutionary modification of developmental processes has been found to often underlie the evolution of the adult phenotype, yet many of the mechanisms by which developmental change leads to phenotypic evolution remain unclear.

Development can evolve in many ways, and alterations to the timing or duration of developmental events, known as heterochronic shifts, are among the best-studied (Raff, 1996). Heterochronic shifts have been found to play a role in the evolution of a broad range of phenotypes such as beak shape across Darwin's finches (Mallarino et al., 2012), bird skulls (Bhullar et al., 2012) and crocodilian snouts (Morris et al., 2019), all of which arose from changes in the timing of cranio-facial development. Similarly, evolutionary changes in developmental pattern formation — heterotypic shifts — also contribute toward generating phenotypic divergence as exemplified by the evolution of limblessness in snakes, which has been driven by spatial changes in gene expression during development (Cohn & Tickle, 1999).

Gene regulatory networks play a central role in establishing the temporal and spatial organisation of developmental patterning, and evolutionary changes in these networks can have profound phenotypic consequences. Heterochronic shifts caused by changes in biochemical network parameters such as protein degradation rates, have been seen to underlie inter-species differences in the tempo of neural differentiation (Rayon et al., 2020) and the frequency of the segmentation clock (Matsuda et al., 2020; Lázaro et al., 2023). Changes to the architecture of gene regulatory networks, including substantial ones such as gene co-option, underpin some of the most striking cases of morphological innovation, such as the evolution of beetle horns and butterfly eyespots (Hu et al., 2018; Murugesan et al., 2022). Recently, attention has turned to the possibility that the evolution of morphogenesis itself — independent of the underlying patterning mechanisms — may also contribute towards phenotypic diversification (Münster et al., 2019; Petridou et al., 2021; Busby & Steventon, 2021; Fulton et al., 2022a; Serrano Nájera & Weijer, 2023), although concrete empirical examples of this are still scarce.

It is well established that modifying the developmental processes patterning adult traits in the embryo often underlies the evolution of phenotypic diversity and novelty. However, how

changes earlier in development might affect phenotypes patterned later remains poorly understood. Developmental processes are tightly coupled in space and time, with each process unfolding from the conditions set by the processes that preceded it. Theory, particularly dynamical systems theory (Jaeger & Monk, 2014; Verd et al., 2014; Crombach et al., 2016; Sáez et al., 2022; Kadiyala et al., 2025), has shown that initial conditions can exert a strong influence over system trajectories, significantly altering the final phenotypic state. Despite this, initial conditions have not yet been explicitly considered an evolvable parameter in developmental evolution in the same way that rates, duration or network architecture have. This gap limits our understanding of how variation arising earlier in development propagates to influence later-forming traits and ultimately contributes to morphological evolution.

Vertebral count is one of the most diverse traits across vertebrates, varying from less than 10 in some frogs to several hundred in snakes, all while being remarkably constant within any given species (Hammond et al., 2025; Bucklow et al., 2025b). Vertebrae develop from somites, paired blocks of mesodermal tissue formed in the early vertebrate embryo on either side of the developing spinal cord (Stickney et al., 2000; Holley, 2007; Oates et al., 2012). Somites are patterned periodically as the vertebrate embryo elongates posteriorly during a process known as somitogenesis (Schröter et al., 2008; Oates et al., 2012; McDaniel et al., 2024). Their formation is preceded by travelling waves of gene expression which sweep across the pre-somitic mesoderm (PSM) from posterior to anterior (Holley, 2007; Oates et al., 2012; McDaniel et al., 2024), providing temporal information that is translated into periodic somite boundaries in the anterior PSM. These waves emerge from a network of coupled genetic oscillators known as the segmentation clock, which drives oscillatory gene expression dynamics at the single cell level and controls the tempo of somite formation (Schröter et al., 2012; Oates et al., 2012; McDaniel et al., 2024).

The position in the anterior PSM at which oscillatory states are converted into stable segmental identities is defined by the wavefront. Originally proposed by Cooke and Zeeman in 1976 as a positional threshold for segment determination (Cooke & Zeeman, 1976), the wavefront has subsequently been suggested to be molecularly implemented by opposing gradients of signalling molecules such as Wnt and Fgf (Oates et al., 2012). More re-

cent work, however, indicates that the wavefront may instead be generated by dynamic FGF–ERK signalling (Niwa et al., 2011; Simsek & Özbudak, 2018), in which oscillatory ERK activity propagates over a posterior-to-anterior signalling gradient driving periodic somite formation (Simsek et al., 2023). As the PSM elongates, the wavefront regresses posteriorly relative to the developing tissue (Cooke & Zeeman, 1976; Aulehla & Pourquié, 2010; McDaniel et al., 2024) leading to the generation of new somites.

While somitogenesis is conserved across the vertebrate tree, the underlying gene expression dynamics and morphogenetic mechanisms vary widely across species. There is a remarkable degree of plasticity in the genetic components of the segmentation clock, and its period differs between species (Krol et al., 2011; Hammond et al., 2025), with recent *in vitro* studies showing up to fourfold differences in mammalian clock periods (Lázaro et al., 2023). The morphogenetic mechanisms driving PSM elongation also diverge across species; patterns of cell rearrangements, motility and proliferation have all been found to be evolvable (Lawton et al., 2013; Bénazéraf et al., 2010; Steventon et al., 2016; Thomson et al., 2021; Mongera et al., 2018; Romanos et al., 2024). Furthermore, the total duration of somitogenesis differs widely between species (Hammond et al., 2025). Together these data illustrate that somitogenesis is a highly evolvable and plastic developmental process, which explains why it has been assumed that its evolution is responsible for the evolution of vertebral counts.

Most of what we know about somitogenesis comes from studies in traditional model organisms such as mouse, chick and zebrafish (Oates et al., 2012; Bénazéraf, 2019). While the study of these systems has been very successful at elucidating general principles and important species-specific differences in somitogenesis, the last common ancestor of these species lived more than 400 million years ago. Divergence of these species over such a long timescale obscures the developmental origins of evolvability: with co-evolution of many developmental processes and the accumulation of neutral changes, it is impossible to tell which processes evolve most readily, and which have causally contributed to changes in vertebral counts. To overcome this limitation, we focus on a closely related species group, the Lake Malawi Cichlid fishes, to study the evolvability of somitogenesis.

Lake Malawi cichlids are a powerful emerging model system in evolutionary developmen-

tal biology (Turner, 2007; Santos et al., 2023). Around 850 cichlid species have evolved in Lake Malawi from a single common ancestor in less than a million years (Malinsky et al., 2018). In this short amount of time, cichlids have colonised every available niche in the lake, exhibiting an astonishing degree of phenotypic diversity in traits such as body shape and size, colour and pattern, cranio-facial morphology, social and breeding behaviours, and vertebral counts which range between 28 and 40 (Bucklow et al., 2025a, 2025b; Santos et al., 2023). In this work, we take advantage of the close relatedness and spectacular diversity of Lake Malawi cichlids to investigate the developmental basis of vertebral count evolution. To do this, we compare somitogenesis in *Astatotilapia calliptera*, the extant Malawi cichlid species thought to most closely resemble the ancestral phenotype of the radiation (Malinsky et al., 2018), which makes 33 ± 1.6~~33~~ somites and 29.7 ± 0.6 vertebrae with *Rhamphochromis* sp. 'chilingali', one of the most elongated species in the lake catchment, which makes 39 ± 1.8~~38~~ somites and 36.5 ± 0.6 vertebrae (Fig. S1, Bucklow et al., 2025b, previously quantified in Marconi et al., 2023), resulting in a 25% difference in somitic counts between the two.

Our results show that somitic counts have evolved without evolving somitogenesis: we find that the tempo of somitogenesis is conserved, as are the mechanisms underlying PSM morphogenesis. Instead, we see that the initial conditions of the process have evolved dramatically, with the PSM being much larger at the onset of somitogenesis in *R.* sp. 'chilingali' than in *A. calliptera*. We see that this difference in the initial size of the tissue is enough to increase the total duration of the process, increasing the total number of somites patterned as a result without the need to evolve somitogenesis itself. Thanks to the short evolutionary distances separating our model species, we provide an empirical example of phenotypic evolution through changes in the initial conditions of a developmental process, rather than through changes to the focal developmental process itself. We propose that this is a generally applicable mechanism of phenotypic evolution, particularly over short evolutionary timescales, and one that may drive early diversification events during speciation.

RESULTS

The duration of somitogenesis differs between *A. calliptera* and *R.* sp. 'chilingali', but the segmentation clock frequency is conserved

We hypothesised that the increased number of somites in *R.* sp. 'chilingali' relative to *A. calliptera* results from an increase in the rate or duration of somitogenesis (Gomez et al., 2008; Hammond et al., 2025). To investigate this, we quantified the total number of somites in embryos of known ages, staged in hours post fertilisation (hpf) (Fig.1.A-M). We found that somitogenesis does not begin at the same time in both species: the first somite in *A. calliptera* appears at ~33hpf, while in *R.* sp. 'chilingali' it appears five hours later, at ~38hpf Fig.(2.B). This indicates that *R.* sp. 'chilingali' embryos take longer to complete earlier stages of development including blastulation and gastrulation, than those of *A. calliptera*. Additionally, we see that somitogenesis takes longer to complete in *R.* sp. 'chilingali' than in *A. calliptera*: Fig.Fig.2.B shows that *A. calliptera* embryos have a full set of somites at 68hpf, while *R.* sp. 'chilingali' will not have the complete set of 39 somites until 80hpf Fig.(2.B). The duration of somitogenesis is therefore increased in *R.* sp. 'chilingali' with respect to *A. calliptera*, taking 42 hours compared to 35; a difference of seven hours.

We measured nascent somite length directly and found it to be broadly similar between the two species, although a subtle difference suggests that this trait may be beginning to diverge (2.C). Nascent somites in *A. calliptera* were consistently slightly longer at the same stage than those of *R.* sp. 'chilingali', with an average difference of approximately ~~2.7~~ 5µm (Fig.2.C). Although the effect size is small (η^2 = 0.05), this observation is consistent with reports from other vertebrate systems in which evolutionary increases in vertebral number are accompanied by reductions in somite size (Seleit et al., 2026). In contrast, nascent somite volume was statistically indistinguishable between species (p = ~~0.82~~ 0.11, two way ANOVA also accounting for somite stage), and decreased over developmental time in both species (Fig. 2.D, p < 0.001; η^2 = ~~0.32~~ 0.53). Together, these results indicate that nascent somite size is largely conserved between the two species, with only a subtle difference in somite length but not in volume, despite their divergent somite numbers.

Thus, despite their divergent somite numbers, the two species show remarkably similar somitogenesis dynamics: somites form at a conserved rate of approximately one every 66 min (0.91 somites·hr^{-1}), and nascent somite size is largely conserved. At this shared rate,

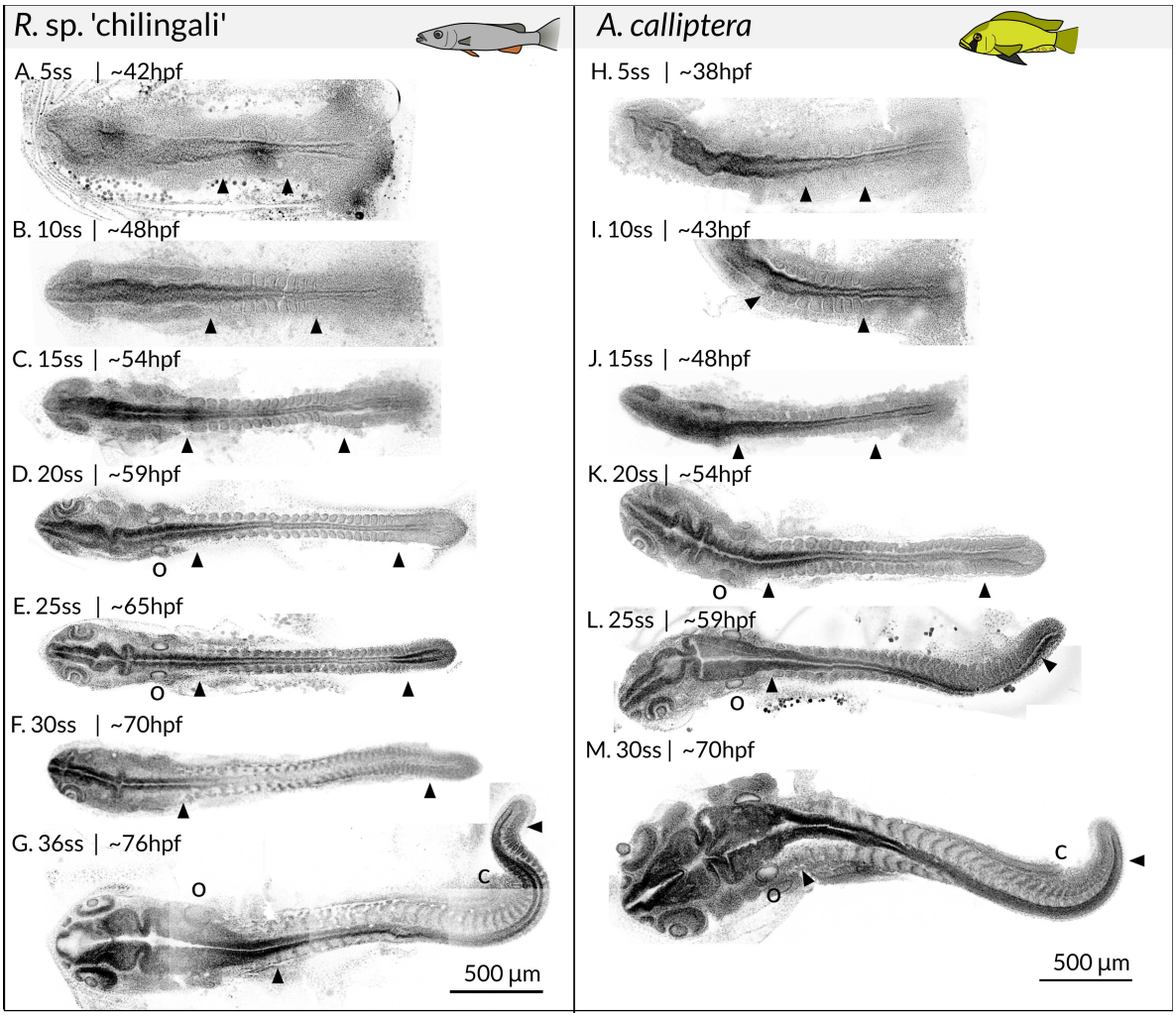


Figure 1: Overview of cichlid somitogenesis. **A-M:** single optical section of flat-mounted DAPI-stained (black) cichlid embryos at different somite stages (ss). Dorsal view, anterior to the left. All embryos are shown on the same scale. Scale bar: 500 µm. Arrows indicate the position of the first and last somite. o: otic vesicle. c: cloaca.

the additional ~7 hrs of somitogenesis in *R. sp. 'chilingali'* is expected to produce ~6 additional somites, closely matching the observed difference in average somite number between the species (39 vs 33). We therefore attribute the elevated somite count of *R. sp. 'chilingali'* primarily to an evolutionary increase in the duration of somitogenesis, rather than a change in its rate or any substantial change in nascent somite size.

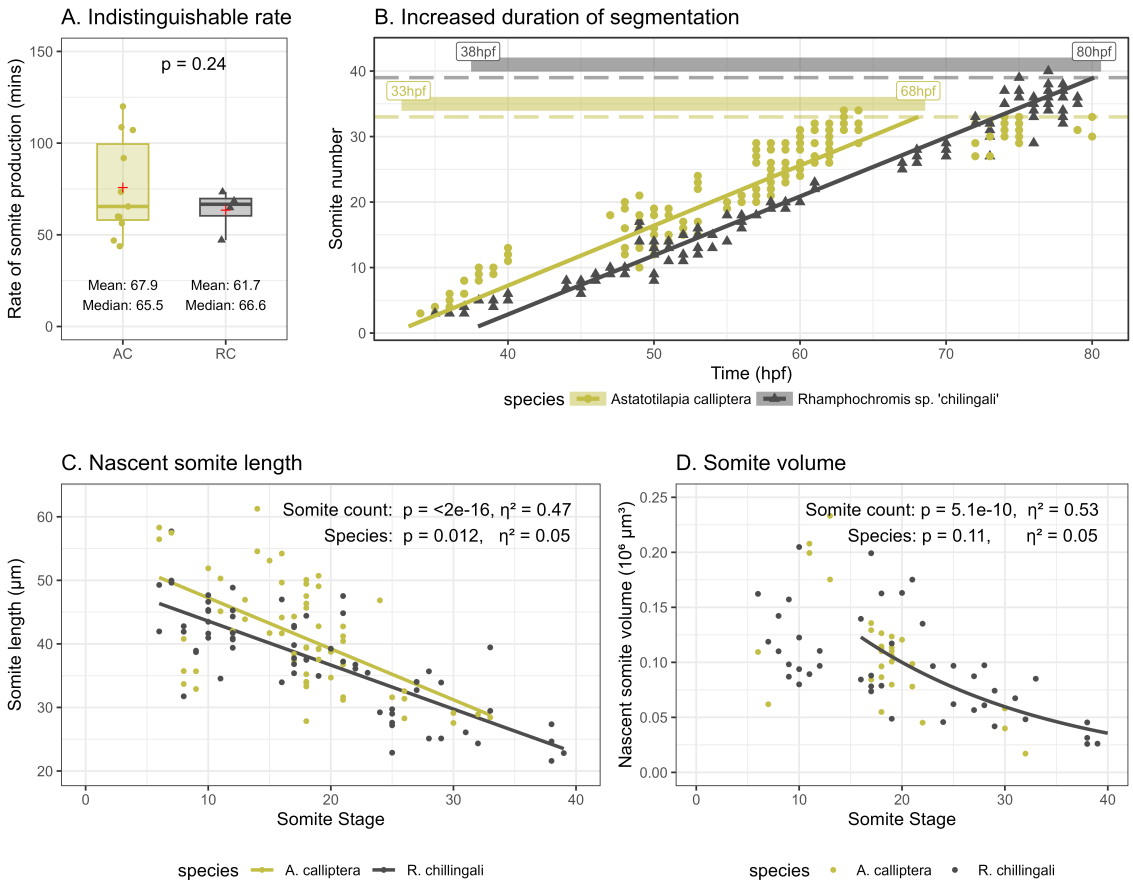


Figure 2: The rate of somitogenesis is conserved between species, while nascent somite dimensions are largely similar. A. Somitogenesis rate in both species, computed for each clutch with more than two timepoints. *A. calliptera* embryos older than 70hpf are excluded from the analysis as they have finished producing somites at that stage. Clutches with limited temporal resolution (data for less than two hours, and less than three samples) were also excluded. See Methods section for details on how the somitogenesis rate was calculated. For this and all subsequent boxplots, the whiskers represent 1.5 times the interquartile range and the box represents the interquartile range (25-75% percentile). The line stands for the median value, and the red cross for the mean. **B.** Number of somites are plotted against time in hours post fertilisation (hpf) in both species, *A. calliptera* is shown in yellow and *R.* sp. 'chilingali' in black. A linear regression was constructed for both species using the segmentation rate calculated in Fig. 1.A, and the intercept was fitted using ordinary least squares. *A. calliptera* somite number = $32.1 + 1.09t$ (one somite formed every 65.5mins). *R.* sp. 'chilingali' somite number = $36.8 + 1.11t$ (one somite formed every 66.6mins), where t is time in hours post fertilisation. Sample sizes: 169 embryos for *A. calliptera* across 11 clutches. 131 embryos for *R.* sp. 'chilingali' across 4 clutches. **C.** *A. calliptera* have longer nascent somites than *R.* sp. 'chilingali'. Nascent somite antero-posterior length, measured from high-resolution confocal images of the PSM, is plotted against somite stage for both species. *A. calliptera* somite length = $55.3 - 0.802ss$ ($R^2 = 0.33$). *R.* sp. 'chilingali' somite length = $50.5 - 0.692ss$ ($R^2 = 0.62$), where ss stands for somite stage. N_{AC} : 70. N_{RC} : 68. (N_{AC}/N_{RC}: sample size for *A. calliptera* and *R.* sp. 'chilingali' respectively). **D.** Volume of the nascent somite is the same between species. N_{AC} : 30. N_{RC} : 44.

PSM size differs significantly at the onset and early stages of somitogenesis between *R.* sp. 'chilingali' and *A. calliptera*

We have shown that *A. calliptera* and *R.* sp. 'chilingali' differ in both the timing of somitogenesis onset and its total duration (Fig.2.A-B), while the rate of the somite addition is conserved between the two species. This suggests that evolutionary changes in the dynamics of the segmentation clock have not contributed to the divergence in somite number between Lake Malawi cichlids, and instead points to the extended duration of somitogenesis in *R.* sp. 'chilingali' as a potential driver of this divergence (Fig.2). To investigate the basis of this difference, we characterised body axis morphogenesis during somitogenesis, focusing particularly on the pre-somitic mesoderm (PSM), the tissue from which somites are produced.

The anatomy of the PSM and the tailbud is similar between the two cichlid species, the only visually remarkable difference lies in the size of the tailbud at early stages of somitogenesis which already by eye appears to be much larger in *R.* sp. 'chilingali' with respect to *A. calliptera* (Fig.3.A-F). We quantified the morphodynamics of the PSM, measuring both PSM volume and the number of cells in the PSM over the course of somitogenesis. We observe that the growth dynamics of this tissue change over time. Prior to 15 somite stage (ss), there is no statistical evidence that the PSM changes in volume over time in either species ~~(p = 0.54~~p=0.40; two way ANOVA testing the interaction between PSM volume and somite count alongside species). After 15ss, the data are well-approximated by an exponential decay curve in both species (Fig.3.H). It appears that prior to 15ss, loss of tissue to the somites is balanced by lateral ingression of cells into the PSM, maintaining a constant PSM volume. A similar period of constant PSM volume has been observed in zebrafish and chick, although this is restricted to a much shorter window at very early stages, prior to 4ss and 6ss, respectively (Gomez et al., 2008). Beyond these stages, PSM volume decreases in zebrafish, whereas in chick it initially increases before subsequently decreasing. This contrasts with the other species surveyed (lamprey, dogfish, mouse, and multiple species of snake), in which PSM volume has not been reported to remain transiently constant at any stage. (Gomez et al., 2008).

A. calliptera and *R.* sp. 'chilingali' differ in PSM size, particularly at early stages of somito-

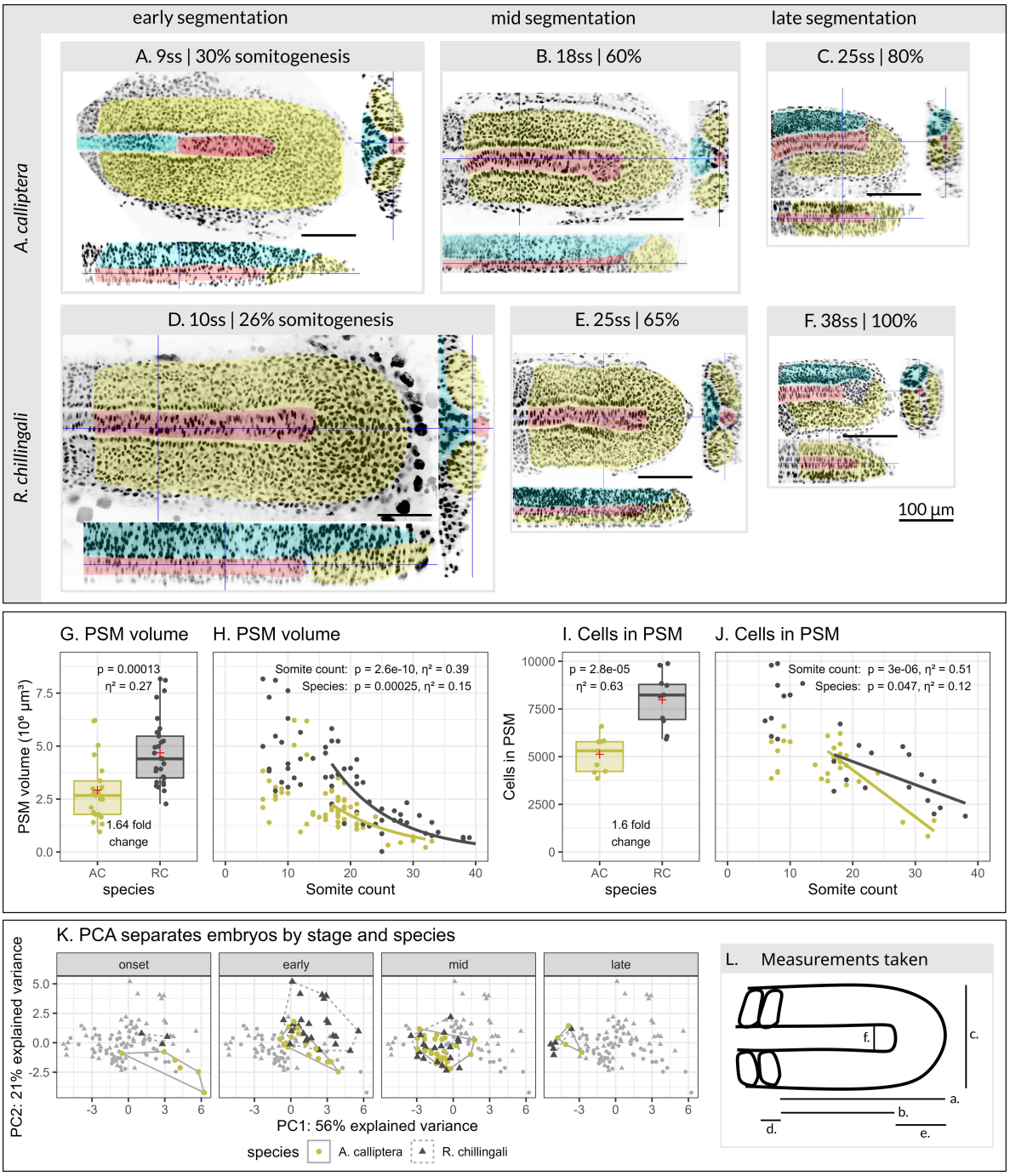


Figure 3: PSM size differs between species only at the onset of segmentation. A-F. Single confocal slices showing the anatomy of the PSM over time in *A. calliptera* and *R.* sp. 'chilingali'. In each panel, the middle image depicts a sagittal slice of the PSM at the level of the notochord; the bottom image depicts a dorso-ventral slice of the PSM through the notochord, from neural tube to notochord, and the right image depicts a dorso-ventral slice of the PSM oriented medio-laterally, at the middle of the PSM. Tissues are false-coloured as follows. PSM: yellow. notochord: red. Neural tube: cyan. DAPI signal is shown in greyscale. Embryos are oriented anterior to the left; scale bar 100µm. All embryos to the same scale. *(Caption continues on the following page.)*

Figure 3: *(Caption continues from the previous page.)* **G.** Quantification of PSM volume for both species 5-15ss. Boxplots represent the upper and lower quartiles of the data, with the solid line representing the median of the data. Red cross represents the mean of the data. Whiskers represent the largest value no further than 1.5 times the inter-quartile range of the plot. N_{AC} : 21. N_{RC} : 29. **H.** PSM volume over the course of somitogenesis. PSM volume was measured manually as described in the Methods section. The trend line was fit to an exponential decay function using nonlinear least squares. N_{AC} : 64. N_{RC} : 63. **I.** Quantification of number of cells in the PSM for both species 5-15ss. Boxplots are laid out as for G. Cells were counted using a custom automatic script described in the Methods. N_{AC} : 9. N_{RC} : 12. **J.** Number of cells the PSM over the course of somitogenesis. The trend line was fit to a linear model using ordinary least squares. N_{AC} : 29. N_{RC} : 28. **K.** Principal component analysis (PCA) of given variables separates species only at early stages of somitogenesis (prior to 15ss). The onset of segmentation is defined as the time before somites epithelialize laterally, 1-5ss. Early segmentation is the period after 5ss but before the PSM separates from the lateral plate mesoderm, 5-15ss. Mid-segmentation is the period post 15ss but before tail eversion: 15-25ss in *A. calliptera* and 15-30ss in *R.* sp. 'chilingali'. Late segmentation is the period between tail eversion and the end of segmentation, 25-33ss in *A. calliptera* and 30-39ss in *R.* sp. 'chilingali'. **L.** Schematic of variables used for PCA. a: PSM length. b: notochord length. c: PSM width. d: nascent somite length. e: Mesoderm progenitor zone (MPZ) length. f: notochord length. Also measured and included were PSM depth, PSM length to width ratio, PSM length to depth ratio, PSM width to depth ratio, and PSM length to somite length ratio. All data points are plotted in grey, and data points for the indicated stage are coloured: (*A. calliptera* yellow, *R.* sp. 'chilingali' grey). N_{AC} : 53. N_{RC} : 53.

genesis. Prior to 15 somites, the volume of the *R.* sp. 'chilingali' PSM is on average ~~61~~64% larger than that of *A. calliptera* (Fig.3.G~~E~~; $p < 0.001$, η^2 = ~~0.25~~0.27, two way ANOVA). After the 15 somite stage, the exponential decay trend lines describing PSM development in both species show that PSM volume remains larger in *R.* sp. 'chilingali' than than *A. calliptera* throughout somitogenesis. This difference is also reflected in PSM cell number: prior to 15 somite stage, the *R.* sp. 'chilingali' PSM has ~~57~~60% more cells than that of *A. calliptera* ($p < 0.0001$, $\eta^2 = 0.63$, Fig.3.J) and this difference persists beyond the 15 somite stage ($p = 0.047$; $\eta^2 = 0.12$, Fig.3.J). *R.* sp. 'chilingali' are consistently larger overall, exhibiting greater embryonic and PSM lengths over the course of somitogenesis (Fig.S3.A-D). However, while the head occupies a similar proportion of embryonic length in both species, the PSM consistently occupies a larger proportion in *R.* sp. 'chilingali' than in *A. calliptera* (FigS3E,G). Thus, the PSM of *R.* sp. 'chilingali' is disproportionately larger than that of *A. calliptera*, even beyond what would be expected from its greater overall embryonic size.

We performed a detailed quantitative comparison of the shape of the PSM over the course of somitogenesis in both species by measuring the dimensions of the different regions in the cichlid unsegmented tailbud: we measured the PSM length, width and depth, the length of the notochord, the length of the putative mesodermal progenitor zone (MPZ), the

nascent somite size, as well as the ratios between these values (11 metrics in total, Fig.3.L). Principle component analysis (PCA) on this dataset separates embryos by stage, with onset of segmentation stage embryos (2-5ss) occupying the lower right quandrant of the graph plotting PC1 and PC2, early stage embryos (5-15ss) in the middle to middle right, mid-somitogenesis embryos (15ss-25ss in *A. calliptera*; 15-30ss in *R.* sp. 'chilingali) are placed in the middle, and late somitogenesis embryos (25-33ss in *A. calliptera*; 30-39ss in *R.* sp. 'chilingali) on the left (Fig.3.K). Importantly, *A. calliptera* and *R.* sp. 'chilingali' cluster together at mid and late stages of somitogenesis, only segregating by species at the onset and early stages of somitogenesis (Fig.3.K), with *R.* sp. 'chilingali' tending towards higher PC2 values than *A. calliptera*. This suggests that the morphometric differences in tailbud shape between species are most pronounced and only significant at the onset and early stages of somitogenesis.

Within species, all tailbud measurements are significantly associated with somite stage (Table S1). After correcting for multiple testing and accounting for somite stage, only PSM length, notochord length, PSM length to somite length ratio, and MPZ length were found to differ between species (Fig.S4, Tables S1, S2). All of these are ultimately a consequence of the larger PSM length in *R.* sp. 'chilingali': notochord length is tightly correlated with PSM length, and the difference in PSM length between species with the conserved somite lengths explains the different PSM length to nascent somite length ratios. Finally, the increased size of the MPZ could indicate a larger pool of progenitor cells in *R.* sp. 'chilingali'.

We next used these data to establish whether species differences are established at the onset and early stages of somitogenesis, or instead involve changes to the process of somitogenesis. If differences in PSM length between species are set at the onset of somitogenesis, we would observe growth curves with different intercepts but similar slopes. Alternatively, if the rate of change in PSM length differed between species throughout somitogenesis, we would see growth curves with differing slopes, potentially pointing at differences in the mechanisms regulating PSM length between species. For all the measurements which differ between species, our data supports the first possibility: the intercept differs, but not the rate of change over the course of somitogenesis. This indicates that the morphogenetic processes are conserved but that the initial conditions have evolved (Fig.S4, Tables S1, S2).

We have shown that PSM dimensions differ most during the onset and early stages of somitogenesis, prior to the 15 somite stage. In particular, we observe that differences in PSM and embryo length are already apparent at the earliest stages of somitogenesis. Between the 1- and 5-somite stages, the PSM of *R.* sp. 'chilingali' embryos is close to 10% longer than that of *A. calliptera* embryos ($p = 0.047$, Figure 4I). This difference increases to 24% between the six- and 15-somite stages, possibly coinciding with a period of continued lateral ingression of presumptive PSM cells as this tissue forms. Total embryo length also differs significantly between species at the 1- to 5-somite stages ($p = 0.0043$, Figure 4I), with *R.* sp. 'chilingali' embryos being 13% longer than *A. calliptera* embryos, and the difference narrowing to 10% through the six- to 15-somite stages. These data show that species-specific differences in embryonic and PSM dimensions arise by and during the early stages of somitogenesis.

Taken together, our analyses show that these two cichlid species differ most markedly at the onset and early stages of somitogenesis. We find that differences in traits such as PSM volume and length, amongst others, are established early in somitogenesis, and possibly before, rather than arising from any species-specific rates of change during somitogenesis. This suggests that while the initial conditions of this developmental process differ between species, the processes driving axial elongation during somitogenesis appear to be conserved in both cichlid species. Our data thus support a scenario in which the increased somite number in *R.* sp. 'chilingali' evolved through changes in initial PSM size, rather than by modifying PSM morphogenesis or axial elongation during somitogenesis.

Both species begin somitogenesis with one somite, and add somites sequentially thereafter.

In order to establish that total somitic counts indeed depend on the size of the PSM at early stages of somitogenesis, it was important to establish whether either species forms significant numbers of segments simultaneously at the onset. We fixed embryos at hourly intervals at early stages of somitogenesis. When obtaining embryos with 0-4 somites for both species, these clearly show that neither species forms any somites simultaneously, consistent with findings in zebrafish and chick (Fig.S5, Fig.S6, Fig.4) (Schröter et al., 2008; Maia-Fernandes et al., 2024). Furthermore, we found no difference in the early versus later

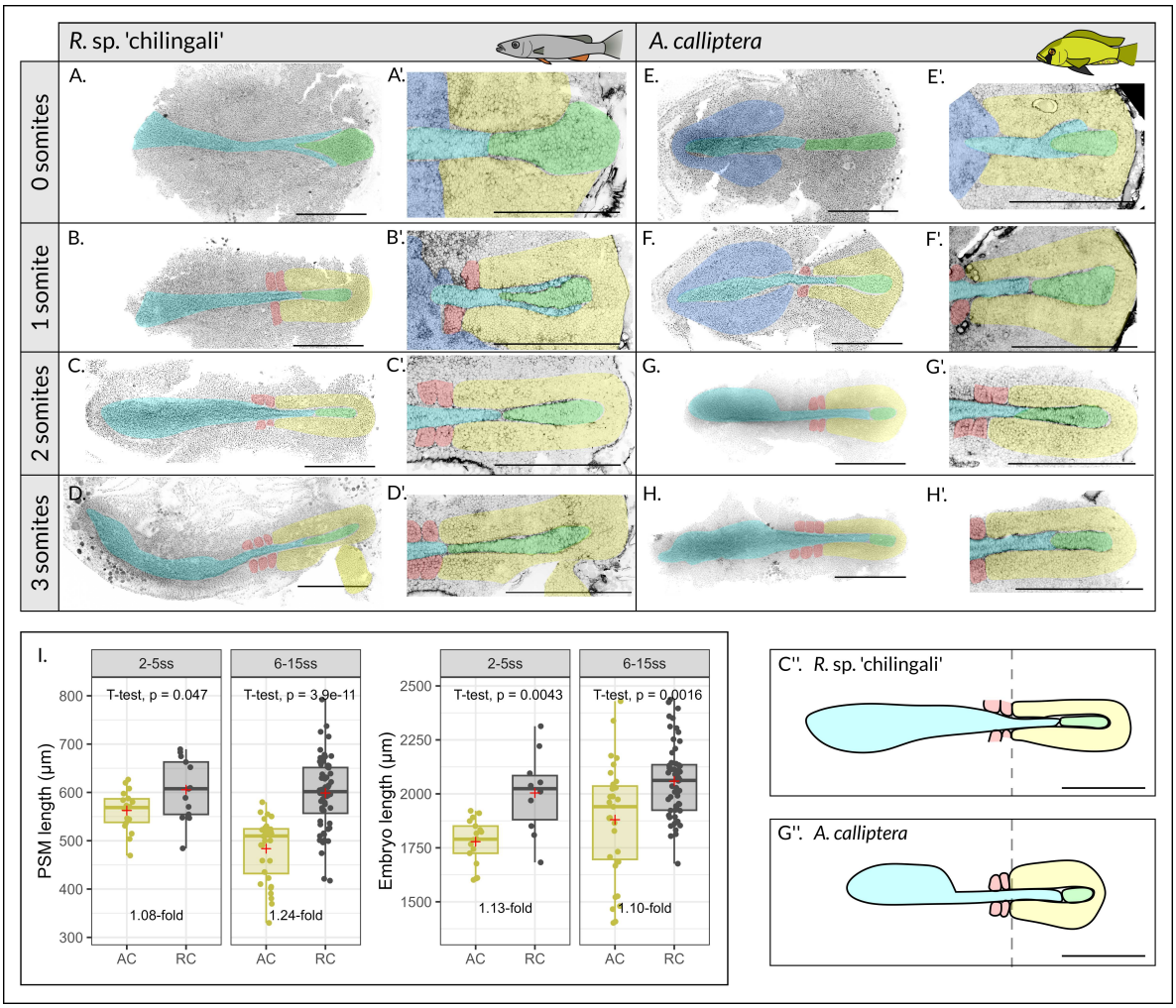


Figure 4: Anatomy of the early embryo and unsegmented region at the onset of segmentation. A-H. Whole-mount, dissected cichlid embryos stained with DAPI (nuclei) and phalloidin (actin). Images to the left (A-H) are shown complete, with nuclei in grey. Images to the right, **A'-H'.** magnify the unsegmented region, and show actin/phalloidin in grey. Individual tissues are false-coloured as follows: neural tube: cyan; notochord and notochord progenitors: green; somites: red; approximation of the unsegmented mesoderm: yellow; ectoderm: dark blue. Scale bar: 500 µm. All embryos are oriented with anterior to the left and are shown in a dorsal view. **I.** PSM and embryo length at the onset of segmentation (2-5ss) and early segmentation (6-15ss). Boxplots are laid out as in Fig.3G & I. 2-5ss: N_{AC} : 18. N_{RC} : 14. 6-15ss: N_{AC} : 32. N_{RC} : 61. **C'', G''**: outlines of embryos in C and G, aligned by the anterior boundary of the PSM, to highlight the differences in size between species. Colour-coded as for A-H.

rates of somitogenesis nor between species: while the breeding behavior of cichlids means that development within a clutch is asynchronous and that there is variation in the number of somites represented at each time-point, it appears that somites also appear approximately once every hour at the onset of segmentation, as they do at later stages (Fig.S5 and Fig.S6).

Despite the fact that *R.* sp. 'chilingali' embryos at the onset of somitogenesis (1-5ss) are older (in hpf) than their *A. calliptera* counterparts, the early anatomy of these embryos is indistinguishable between both species. Compared to embryos at later stages of somitogenesis, in early somitogenesis the PSM appears morphologically continuous with the lateral plate mesoderm, and somites have not yet epithelialised laterally (compare Fig.4 and Fig.3.A-F). The only obvious difference between species lies in the overall size of the embryo and in particular, of the PSM, where as already shown above, the PSM in *R.* sp. 'chilingali' is bigger than in *A. calliptera*. These data further support the notion that it is the initial size of the PSM that determines total somitic counts, and that species-specific differences in PSM size are established prior to the onset, and at the early stages of somitogenesis.

The molecular anatomy of the tailbud is indistinguishable between species

To test whether the observed similarities in PSM morphodynamics were reflected at the molecular level we characterized the expression of genes known to be important for PSM morphogenesis and somite patterning across vertebrates in both *A. calliptera* and *R.* sp. 'chilingali'. These included the gene *tbxta*, which is required for the specification both of the notochord and the posterior body in vertebrates (Schulte-Merker et al., 1992, 1994; Martin & Kimelman, 2008, 2010). As in other vertebrate embryos studied, *tbxta* is expressed in the notochord both in *A. calliptera* and *R.* sp. 'chilingali', as well as in the germ ring in early embryos (Fig.5A', B', D', E'). At early and mid stages of somitogenesis, *tbxta* is expressed in the notochord and in the posterior-most region of the PSM. *tbxta* expression is similar between species, and indistinguishable when quantified at early and mid segmentation (Fig.5A', B', D', E', F).

The genes *tbx16* and *msgn* are required for correct cell motility patterns in the zebrafish tailbud, where they are expressed in a posterior-to-anterior gradient (Manning & Kimelman,

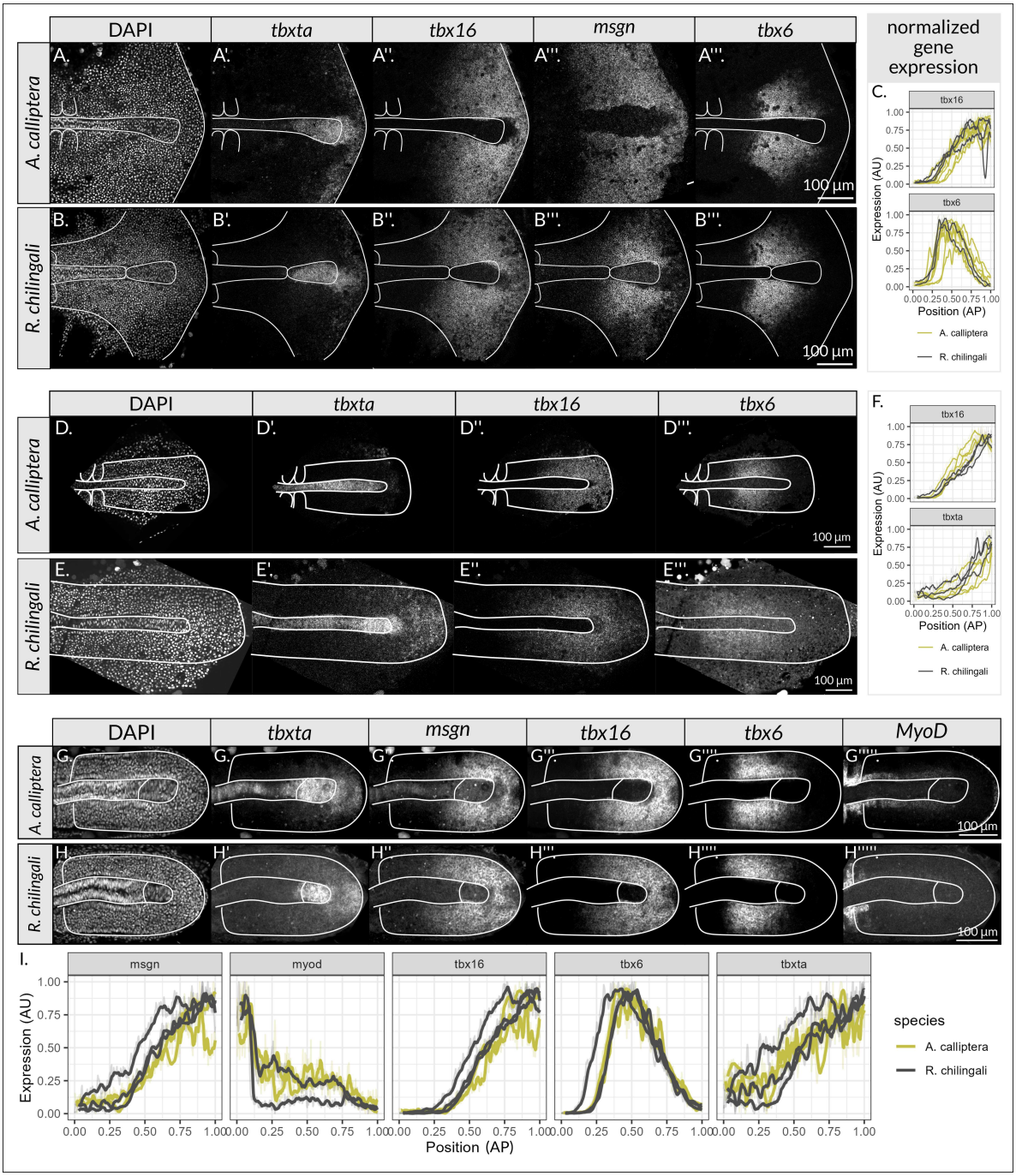


Figure 5: Patterning of the PSM is indistinguishable between species. A-B. Single confocal sections of very early somitogenesis stage embryos (3ss) simultaneously stained for DAPI, *tbxta*, *tbx16*, *msgn*, and *tbx6*. Scale bar: 100μm. Thick white lines outline the nascent somites, notochord, neural tube, and unsegmented region boundary. **C.** Normalized gene expression measured across multiple embryos. Length and amplitude normalisation performed as described in the Methods section. In brief, *tbx6* and *tbx16* expression is measured along the middle of the PSM and across the same line for each gene. N_{AC} : 6. N_{RC} : 2. **D., E.** Single confocal sections of early somitogenesis stage embryos (9-10ss) simultaneously stained for DAPI, *tbxta*, *tbx16*, and *tbx6*. Scale bar: 100um. Thick white lines outline the nascent somites, notochord, neural tube, and unsegmented region boundary. *(Caption continued on the following page.)*

Figure 5: *(Caption continued from the previous page.)* **F.** Normalized gene expression measured across multiple embryos, as in C. **G-H.** Single confocal sections of mid-segmentation stage embryos stained simultaneously for DAPI, *tbxta*, *tbx16*, *msgn*, *tbx6*, and *MyoD*. Thick white outlines outline the PSM, notochord, and neural tube. **I.** Quantifications of spatial gene expression for each gene at mid somitogenesis stages, normalised as described in the Methods section. The spatial expression of *tbxta*, *tbx16*, *msgn*, and *tbx6* was measured along the same line, across the midline of the embryo. The expression of *MyoD* is measured along the adaxial layer of cells. $N_{AC} = 2$. $N_{RC} : 3$. *A. calliptera* are 20ss or 60% somitogenesis, *R.* sp. 'chilingali' are 25ss or 65% somitogenesis. All embryos are oriented anterior left and shown in a dorsal view. Different channels of the same embryo are shown in each row, except for **A""**.

2015). This expression pattern is conserved in cichlids, and when quantified, the slope and position of the expression domain is indistinguishable between both species at early and mid-segmentation (Fig.5A", B", A"', B"', C, D", E", F, G", H", G"', H"', I). The gene *tbx6* is required for somite specification (Nikaido et al., 2002; Ban et al., 2019), and in *R.* sp. 'chilingali' and *A. calliptera* it is expressed in a broad domain of gene expression in the anterior PSM, as expected, with a sharp anterior boundary and a more shallow posterior boundary, similar to the pattern that has been reported in zebrafish (Nikaido et al., 2002; Ban et al., 2019) (Fig.5A"', B"", C, D"', E"', G"", H""). As with the other genes quantified, spatial expression of *tbx6* in the PSM is indistinguishable between both cichlid species at early and mid segmentation stages.

Finally, *MyoD* is involved in muscle development in the newly formed somites (Weinberg et al., 1996; Osborn et al., 2020), and is expressed in nascent somites and in a single row of cells directly adjacent to the notochord - the adaxial cells - in both species (Fig.5.D"", E"", F). When quantified, the expression of this gene, like that of all other genes characterised, is also indistinguishable between the two cichlid species.

Altogether, our data indicate that *A. calliptera* and *R.* sp. 'chilingali' do not differ in the molecular patterning of the PSM at early or mid segmentation stages. This supports the notion that the molecular mechanisms underlying the development of the PSM during somitogenesis are conserved in these species.

DISCUSSION

Lake Malawi cichlids have evolved increased somitic counts by modifying the initial conditions of somitogenesis

Altogether, our results indicate that *R.* sp. 'chilingali' has evolved an increased number of somites by altering the initial conditions of somitogenesis rather than by modifying the process of somitogenesis itself. While *R.* sp. 'chilingali' and *A. calliptera* differ in the duration of somitogenesis, which takes seven hours longer in *R.* sp. 'chilingali' than in *A. calliptera*, the rate of somitogenesis is conserved between the two (Fig.1.N&O). Furthermore, somites were found to form sequentially throughout somitogenesis in both species, with no evidence of simultaneous formation of somites or a difference in the rate of somitogenesis, even at the onset of somitogenesis (Fig.4).

Our results contrast with those reported by Marconi and colleagues, who identified a statistically significant increase in somitogenesis rate in *R.* sp. 'chilingali' relative to *A. calliptera* (68 minutes per somite in *R.* sp. 'chilingali' and 74 minutes per somite in *A. calliptera*), together with a conserved duration of somitogenesis of ~35 hrs in both species (Marconi et al., 2023). As these estimated rates and durations alone could not fully account for the observed difference in somite number between the two species, Marconi *et al.* proposed that the earliest somites may form simultaneously in Lake Malawi cichlids, rather than sequentially. This interpretation was informed by their experimental observations, in which embryos with fewer than four somites were not recovered in either species (Marconi et al., 2023). Here, we directly observe embryos with one, two, and three somites in both species, demonstrating that the earliest somites are added sequentially rather than simultaneously.

The difference between the two studies may therefore reflect differences in how developmental time was defined and how the earliest stages of somitogenesis were sampled. Marconi *et al.* estimated the onset of somitogenesis using the appearance of the neural keel as a developmental landmark and determined somite number at subsequent time points (Marconi et al., 2023). In contrast, we measure developmental time continuously from fertilisation, allowing the one-, two-, and three-somite stages to be positioned directly within the developmental time course and incorporated into estimates of the timing and rate of somite formation. Notably, our estimate of the somite addition rate in *R.* sp. 'chilingali' differs from that of Marconi *et al.* by only 2 minutes per somite, whereas the corresponding

estimates for *A. calliptera* differ by 12 minutes per somite. Given the small absolute magnitude of these discrepancies, differences in temporal resolution and the representation of the earliest stages may be sufficient to account for the variation in the estimates between the two studies. Importantly, our data resolve the earliest stages of somitogenesis as a sequential process and support a largely constant rate of somite addition throughout somitogenesis in both species (Fig. 1N).

We have shown that the early *R.* sp. 'chilingali' PSM is significantly larger than that of *A. calliptera* in every dimension measured, being 19% longer, ~~61~~ 64% greater in volume, and having ~~57~~ 60% more cells (Fig.3). Despite these significant initial differences in PSM size, PSM growth rates are indistinguishable between both cichlid species (Fig.3), as are the expression patterns of key molecular regulators of PSM morphogenesis (Fig.5), while nascent somite size is largely comparable (Fig.2.C.). Together, these observations indicate that the dynamics of the molecular clock and the morphogenetic processes underlying somitogenesis are conserved, and that it is only the initial conditions in the form of the size of the PSM at the beginning of this process, that have diverged.

If the segmentation clock dynamics or associated morphogenetic mechanisms had diverged, we would expect alterations in PSM anatomy, molecular patterning, and/or growth trajectories; however, none are observed. Even when metrics differ in absolute size (e.g. PSM length, MPZ length), developmental trajectories over time are parallel, reinforcing the interpretation that initial conditions, rather than process, have evolved (Fig.3 and Fig.S3). Therefore our data suggest that the additional tissue required to generate more somites in *R.* sp. 'chilingali' is already present before somitogenesis begins. They support a model in which the extended duration of somitogenesis, and the resulting increase in vertebral number relative to *A. calliptera*, is driven by interspecific differences in PSM size established prior to somitogenesis, rather than by the divergence in any of the mechanisms underlying the process itself.

Importantly, our data show that these interspecific differences are already established prior to somitogenesis. *R.* sp. 'chilingali' initiates somitogenesis later than *A. calliptera*, suggesting an early heterochronic shift during blastulation or gastrulation (Fig.2). An extended pre-segmentation period could permit increased cell proliferation, resulting in a larger em-

bryonic axis at the onset of somitogenesis. However, the PSM in *R.* sp. 'chilingali' is still disproportionately larger than that of *A. calliptera*, failing to scale with embryo size and suggesting a PSM-specific divergence in the mechanisms responsible for the specification of this tissue (Fig.S3). In addition to a larger PSM domain specified during gastrulation, increased lateral ingression during early segmentation stages could also contribute to the larger PSM size in *R.* sp. chilingali. Species-specific differences in proliferation rates before and shortly after the onset of somitogenesis should also be examined in future studies.

Whole-embryo transcriptomic data for these species further support our interpretations by revealing that the largest inter-specific differences occur at the four-somite stage, near the onset of segmentation (Marconi et al., 2024), becoming more similar thereafter. Together, these findings indicate that divergence between these species is most pronounced at the onset of somitogenesis, supporting the view that somitic counts have evolved by evolving the initial conditions of somitogenesis and suggesting that evolutionary differences in other phenotypic traits may likewise be established during the earliest stages of embryonic development.

While our results identify divergence in the initial conditions of somitogenesis as a novel developmental basis for its prolonged duration in *R.* sp. 'chilingali', prolonging somitogenesis itself is a well-established evolutionary route to increasing vertebral number. However, in previously studied systems, prolonged somitogenesis has been achieved through a variety of other developmental mechanisms. In snakes, high vertebral number has evolved through a combination of accelerated somite formation and prolonged somitogenesis (Gomez et al., 2008; Hammond et al., 2025), while in anguilliform eels, prolonged somitogenesis is associated with the extended maintenance of axial progenitors in the tail (Kawakami et al., 2017; Seleit et al., 2026). Similarly, vertebral number has evolved over ~10,000 years in the Deer mouse *Peromyscus maniculatus* by changing the duration of somitogenesis, achieved by altering the proportion of axial progenitors in the tail (Kingsley et al., 2024).

Altering the duration of somitogenesis may in general present an easier route for evolution to change vertebral number. Assuming that the timing of Hox gene activation is unchanged relative to the start of somitogenesis, prolonging somitogenesis would only change the number of vertebrae in the caudal part of the body. In contrast, globally changing the

number of vertebrae by altering the frequency of somitogenesis (Harima et al., 2013) may have deleterious effects, for example in carnivorous mammals, where a specific number of presacral vertebrae and the resulting spinal flexibility are required for fast running (Galis et al., 2014). Our results suggest that while prolonging somitogenesis may represent a common developmental route to increasing vertebral number, this can evolve through substantially different developmental mechanisms, including, as we show here, through changes to the initial conditions of somitogenesis.

Evolution can be driven by changes in the initial conditions of developmental programs

Our findings highlight an additional route by which phenotypic evolution can occur. Phenotypic evolution need not be rooted in the modification of the underlying focal developmental process itself, but rather in changes to its initial conditions. Instead of modifying a complex developmental process, such as somitogenesis and axial elongation, it may be simpler to instead evolve the initial conditions of that process, particularly over shorter timescales. These potentially subtle changes early on in embryogenesis can cascade through development giving rise to dramatic consequences for the adult phenotype. In the context of the evolution of vertebral counts in Lake Malawi cichlids we have shown that these initial conditions correspond to the initial size of the body axis, and of the PSM in particular.

This perspective is complementary to the established idea that evolutionary changes in progenitor populations can drive phenotypic diversification. Perhaps the best-characterised example is mammalian neocortical evolution, where expansion of neural progenitor populations contributes to increased neuronal output and cortical size (Florio & Huttner, 2014; Pinson & Huttner, 2021; Vaid & Huttner, 2022). Comparative cerebral organoid studies have provided experimental support for this idea, demonstrating that subtle differences in the proliferative behaviour of neural progenitors between humans and other great apes are sufficient to generate developmental differences consistent with neocortical expansion (Mora-Bermúdez et al., 2016; Giandomenico & Lancaster, 2017). In these systems however, unlike in cichlid somitogenesis, evolutionary changes in progenitor populations are accompanied by changes in downstream developmental processes, including progenitor

proliferative behaviour and neurogenesis.

The concept of developmental initial conditions may also provide a useful framework for interpreting evolutionary systems in which phenotypic divergence arises through developmental changes occurring prior to the onset of a focal developmental process. The two-tailed goldfish has evolved a second tail by altering dorso-ventral patterning at the gastrula and tailbud stages, driven by a mutation to the gene chordin which arose during artificial selection (Abe et al., 2014). This morph exhibits delayed blastopore closure relative to single-tailed goldfish, and has a larger PSM, which interestingly has resulted in the evolution of two tails rather than increased vertebral counts (Abe et al., 2014; Li et al., 2019).

Heterochronies during gastrulation in the Mexican cavefish, *Astyanax mexicanus*, have been found to generate organizer, and interestingly, axial mesodermal tissues with diverging gene expression patterns (Torres-Paz et al., 2019). These differences have been postulated to have contributed towards the divergence in brain evolution between cave and surface morphs. In that work, authors founds that these differences depended fully on maternal factors, and that certain traits such as retinal morphogenesis, retained significant maternal influence throughout development and well into the larval stages. Since cave and surface forms are morphs of the same species, the maternally inherited differences identified in this system provide a particularly clear example of variation in developmental initial conditions from which subsequent developmental processes proceed. It is possible therefore, that in the closely related Lake Malawi cichlids, maternal factors also play an important role affecting early stages in embryogenesis, cascading on during development, affecting downstream processes and manifesting in adult traits.

Unless these differences are entirely driven by differences in maternal inputs, modifying the initial conditions of a focal developmental process will require evolutionary changes in earlier development. For example, although we have shown that somitogenesis itself has not changed between our two species, earlier development has indeed evolved, with *R.* sp. 'chilingali' taking five hours longer to reach the onset of somitogenesis than *A. calliptera* (Fig.1.N; previously shown in Marconi et al., 2023). Our use of the term *initial conditions* is therefore relative to the developmental process under consideration: the focal developmental process. The distinction we make is not between development and non-

development, but between evolutionary changes occurring within a focal developmental process and changes to the developmental context from which that process begins. In this case, we show that evolutionary change occurred in developmental events preceding somitogenesis, altering the state of the embryo at the onset of segmentation while leaving the mechanisms of somitogenesis conserved, yet still leading to a significant change in the number of somites produced. This demonstrates that evolutionary change in upstream developmental processes can drive diversification without requiring modification of the focal developmental process from which the phenotype emerges.

The end of somitogenesis corresponds to the phylotypic stage in vertebrates, also known as the pharyngula stage. This is the stage when vertebrate embryos across species most resemble each other both morphologically (Baer, 1828) and transcriptionally (Irie & Kuratani, 2011). These striking similarities are believed to reflect the developmental stages of most constraint, which may be underpinned by the obligate and deeply conserved progressive expression of the hox genes (Duboule, 1994). Given this deep evolutionary conservation and strong constraints on the morphology of the embryo after segmentation, perhaps the easiest way to evolve vertebral counts over short evolutionary timescales might require bypassing any changes to somitogenesis and any other processes that might take place close to the phylotypic stage, in favor of changes to the initial conditions of these processes.

Finally, changing initial conditions might not be the only way to evolve a phenotype without modifying the underlying developmental process that generates it. Boundary conditions, which dictate how a system interacts with its spatial or structural environment, might also evolve and affect the outcome of conserved developmental processes. It has been proposed that changes in tissue tectonics - or how tissues develop relative to each other - might be enough to vary the placement of signalling centres and responding tissues, potentially resulting in changes to the coordinated timing of development (Blanchard et al., 2009; Busby & Steventon, 2021) that could lead to phenotypic evolution. The effect of boundary conditions is well illustrated in two-dimensional stem cell colonies (Rombouts et al., 2023), where the geometry of the micro-patterns used has been seen to modify the position of primitive streak-like regions, as well as the direction and symmetry of cell migration (Warmflash et al., 2014; Etoc et al., 2016; Heemskerk et al., 2019). Furthermore, it has been shown

that altering geometry and boundary conditions in embryos by modulating the spatial distribution of forces, flows, and active processes - such as through changes in the position of cell ingression - can shift between the different modes of gastrulation described across vertebrates (Serrano Nájera et al., 2025; Serrano Nájera & Weijer, 2023; Chuai et al., 2023; Serrano Nájera & Weijer, 2023). Heterochrony in the expression of "timer genes" controlling how arthropod segmentation gene regulatory networks are deployed within the embryo is also thought to account for the variation in segmentation modes in arthropods (Clark et al., 2019; Clark & Peel, 2018; Taylor & Dearden, 2022), another example of how boundary conditions can shape developmental processes. Taken together, this suggests that boundary conditions, alongside initial conditions as demonstrated in this study, may represent an important and currently underappreciated driver of phenotypic evolution.

CONCLUSION

We have shown that *R.* sp. 'chilingali' have likely evolved increased somitic counts by modifying the initial conditions of somitogenesis, rather than the process of somitogenesis itself. *R.* sp. 'chilingali' have a significantly larger PSM than *A. calliptera* at the onset and early stages of somitogenesis, providing the excess tissue used to produce more somites. Moreover, there is no evidence for a change in the process of somitogenesis between species; the rate of somitogenesis is conserved and morphometric analyses of the anatomy and patterning of the PSM have revealed that these are very similar between *R.* sp. 'chilingali' and *A. calliptera*. This work demonstrates an alternative mechanism by which phenotypic evolution can be achieved, showing that altering the initial conditions of development can result in dramatic phenotypic changes, without the need to modify the underlying developmental process. This mechanism might be particularly useful over short evolutionary timescales or when a developmental process is highly constrained, as could be the case with somitogenesis. We hope our work will encourage others to look for alternative developmental drivers of evolutionary change in closer related species to reveal how phenotypic evolution first emerges.

METHODS

Animal husbandry

A. calliptera and *R.* sp. 'chilingali' were reared at 26°C, under a 12:12 hour day-night cycle. *A. calliptera* were fed JBL Novo Malawi flake (for algae-eating cichlids), and *R.* sp. 'chilingali' were reared on JBL Novo Malawi flake for carnivores. Feed was supplemented with pellets, frozen brine shrimp, and frozen fish for enrichment and to encourage breeding.

Extraction of cichlid embryos

Embryos were extracted from stock tanks at least weekly. Embryos were removed from mouthbrooding females by first catching the female, and then flushing the mouth with water using a plastic pasteur pipette until all embryos were released. All animal work was conducted following approval by the Departmental Animal Welfare Ethical Review Body (AWERB) for the Department of Biology at the University of Oxford.

Estimating the rate of somitogenesis

To establish the rate of somitogenesis, embryos were staged in hours post fertilisation (hpf) by monitoring breeding tanks hourly for the appearance of new mouthbrooders. Alternatively, if a clutch of one-cell embryos was extracted during regular fish husbandry work, the time of extraction was treated as the estimated time of fertilisation. If breeding was observed then fish were left for the duration of courtship (~1.5 hrs) and then embryos were extracted, with the end of courtship treated as the time of fertilization. As the first division takes ~1-2 hrs (Fujimura & Okada, 2007; Marconi et al., 2023), these collection methods are equivalent.

Embryos were cultured in 50 mL Falcon tubes containing ~30 mL of a solution of tank water and 1 mg/L of methylene blue (Sigma-Aldrich) to prevent mould and bacterial contamination. Embryos were incubated on a slow rocker at 26°C. Water was changed and dead embryos removed daily. Once a desired stage was reached, embryos from that clutch were fixed every 1-2 hours in batches of 3-5 embryos. Fixation was performed overnight at 4°C, in 4% v/v formaldehyde (Sigma). Fixed embryos were dissected off the yolk and stained overnight in 1 µL/mL DAPI at 4°C to better resolve the somites, which we found challenging to count otherwise in fixed specimens. DAPI-stained embryos were mounted in glycerol and somites were counted by eye using a Leica MZ FLIII fluorescence stereomicroscope.

The rate of somitogenesis was measured for each clutch by performing a linear regression linking somite stage to hours post fertilization (Fig S2). The slope of this linear regression was taken as the rate of somite production. *A. calliptera* embryos older than 70 hpf were excluded from our analysis, as these embryos have completed somitogenesis. We also excluded clutches with less than three time points. Since our staging method leaves a ~2 hr uncertainty as to the exact age of a clutch, and because clutches were sampled unevenly across time, we computed the species-typical somitogenesis rate as the median of the clutch-specific rates for that species. To estimate the start and end of somitogenesis in each species, we constructed a linear regression, fixing the slope as this inferred species-typical rate.

Hybridization chain reaction

Hybridization chain reaction (HCR) was performed as per (Choi et al., 2016, 2018; Fulton et al., 2022b). Probes were designed by Molecular Instruments; accession numbers for genes can be found in Table 1. In short, embryos were fixed overnight at 4°C in 4% formaldehyde and then dehydrated in a 25%, 50%, 75% methanol:Phosphate Buffered Saline (PBS) series, leaving tissue to equilibrate for five minutes for each methanol concentration. Embryos were then stored at -20°C in 100% methanol. Note that all washes performed are for five minutes unless indicated otherwise.

Table 1: Genes used in this study

Gene name	NCBI accession
tbxta	XM_026157450
tbx16	XM_026187037
tbx6	XM_026153614
sox2	XM_026147476.1
myoD	XM_026172524.1
msgn	XM_026142939

To perform the HCR, embryos were first rehydrated in a 75%, 50%, 25% methanol:PBS series as before. Embryos were then dissected from the yolk in PBS, and placed in a glass staining dish. Permeabilization with proteinase K was typically not required for these stages. If permeabilization was required, embryos were permeabilized for one hour in 10 µg/mL proteinase K (Sigma) before being washed twice in PTw and re-fixed in 4% formaldehyde for

30 minutes.

Embryos were pre-hybridized for 30 minutes at 37°C in 30% hybridization buffer (Molecular Instruments), before 1 µL of probe was added per 100 µL of hybridization buffer. Note that to ensure strong and consistent staining we used ~100 µL of hybridization buffer per half-dozen embryos, and did not stain more than ~15 embryos per staining dish. The embryos were then left overnight to hybridize at 37°C.

The following day, we washed out the probe using 4x15 minute washes in probe wash buffer (Molecular Instruments) at 37°C. At room temperature, we performed 3x5 minute washes in SCT (5X SSC + 0.1% Tween-20), before pre-amplifying in amplification buffer (Molecular Instruments). We heat-shocked the hairpins at 95°C for 90 seconds in separate PCR tubes, before adding these to the embryos. Embryos were then incubated overnight, in the dark.

The following morning we washed out the hairpins in SSCT and added 1 µL/mL DAPI at least overnight at 4°C, before mounting in 90% glycerol and imaging.

Phalloidin staining

Embryos were extracted and fixed as above, before being washed three times in PTw and dissected. Embryos were then permeabilized for a total of two days in 1% PTx, washing four times over this time period. Embryos were then washed three times in PTw before being stained overnight in half a unit (10 µL) Phalloidin-CF568 (Biotin, BT00044-T) in 100 µL PTw and 0.5 µL DAPI (Biotin, BT40011). Finally, the stain was washed out three times in PTw, before embryos were mounted in 90% glycerol.

Imaging

Imaging was performed on either an Olympus FV3000, Leica LSM980, or Leica LSM880. Microscope configuration is summarized in Table 2

Table 2: Microscope configuration

Microscope	Low magnification objective	Medium magnification	High magnfication objective	Lasers (nm)
Olympus FV3000	Olympus UPLSAPO 4X (0.16NA dry)	N/A	UPlanSApo 30x silicon oil (1.05NA)	405, 488, 514, 561, 594, 631
Leica LSM980	Zeiss 10x (0.45 NA Dry)	N/A	40x (1.30 NA Oil)	405, 488, 514, 561, 639
Leica LSM880	Zeiss 10x (0.45 NA Dry)	Plan-Apochromat 20x/0.8 M27	40x (1.30 NA Oil)	405, 488, 514, 561, 639
Leica Stellaris 8	HC PL FLUOTAR 10x (0.30 NA Dry)	HC PL APO CS2 20x (0.75 NA water/multi-immersion)		White light laser

Morphometrics

For the purposes of our morphometric analyses, we define the stages of somitogenesis as follows. Onset of segmentation (1–5ss): the period before somites epithelialize laterally. Early segmentation (5–15ss): the period between complete epithelialization of the nascent somite and full lateral epithelialization of the PSM, when the PSM separates from the lateral plate mesoderm. Mid-segmentation: the period after 15ss but prior to tail eversion (15–25ss in *A. calliptera* and 15–30ss in *R.* sp. 'chilingali'). Late segmentation: the period between tail eversion and the end of segmentation (25–33ss in *A. calliptera* and 30–39ss in *R.* sp. 'chilingali').

We define the extent of the PSM using morphological landmarks. At mid- and late-segmentation stages (15ss and later), PSM volume comprises all tissue within the tailbud, excluding the notochord, neural tube/spinal cord, nascent somites, and hypochord. At early segmentation stages (5–15ss), the PSM is defined in the same way, with its lateral extent taken to be equivalent to that of the somites, consistent with the observed restriction of *tbx6* to this region. The anterior boundary of the PSM corresponds to the posterior boundary of the nascent somite. We consider the nascent somite to have formed once its posterior boundary is fully epithelialized, as determined by the arrangement of nuclei. The anatomical boundaries of the PSM, as defined here, are shown in Figs 3–5.

Because somite formation is a gradual process, determining when a somite is "fully formed"

is necessarily somewhat subjective. Here, we define a somite as fully formed once its posterior boundary is fully epithelialized, as identified by the arrangement of nuclei. To minimise variability in applying this criterion, all measurements were performed by the same researcher throughout the study.

Morphometric measurements were performed by manually annotating images within OMERO (Burel et al., 2015). Variables were defined as follows: The PSM length is defined as the distance between the posterior-most tip of the PSM, at the level of the notochord, and the posterior boundary of the nascent somite; measured through the notochord. The notochord length is the distance between the posterior boundary of the nascent somite, and the posterior tip of the notochord, measured through the notochord. The MPZ length is the difference between PSM and notochord length. Somite length is defined as the distance between the posterior and anterior boundaries of the nascent somite, measured at the middle of the somite. PSM width was measured by placing two points at the intersection of the posterior boundary of the nascent somites, and the lateral aspect of the PSM, and by computing the euclidean distance between these points in Python. PSM depth was measured similarly, at the posterior tip of the notochord, using points placed at the first and last PSM frames. In effect these measurements corresponds to the anterior PSM width and posterior depth and therefore represent proxy measurements. These proxies are accurate at later stages in somitogenesis, where PSM width and depth are roughly constant throughout the antero-posterior length of the tissue. At early segmentation stages however, these lead to underestimates of PSM width in particular, as the PSM widens towards the posterior (Fig 4, Fig 5A,B). Notochord width is measured at the middle of the notochord. The embryo length was measured as a poly-line across the AP axis of the embryo, from the tip of the nose to the tip of the tailbud, following the embryonic spinal cord. Metrics are shown illustrated in Fig.3L.

Principal component analysis was performed in R v4.4.2 using the ‘prcomp‘ command from the ‘stats‘ package, scaling data to have unit variance prior to the PCA being performed.

Manual tissue segmentation

Tissues were manually segmented using the Segmentation Editor tool in ImageJ (Schindelin et al., 2012). The whole tailbud was first outlined every 5-10 slices, then the labels were interpolated and the label added to the image. The notochord, neural tube, and somites were then segmented using the same method, and given unique labels for identification.

To measure the volume of different tissues, the label object was resized so that each voxel measured 1 μm^3. The number of voxels in each label were then counted. For somites, the number of somites segmented (one or two) was detected automatically by extracting the somite label, labeling each somite, and then counting the number of labels. The mean somite volume was then computed by dividing the total somite volume by the number of somites.

Measuring spatial molecular patterns across the AP axis

Gene expression patterns across the anterior-posterior axis were measured in Fiji as follows. First, an average intensity projection of relevant focal planes was performed in ImageJ. Average intensity projections were always performed on focal planes adjacent to the notochord. A polyline was then drawn across the PSM, from the posterior boundary to the nascent somite to the posterior of the notochord, following the middle of the PSM. Expression intensity was then measured, averaging across 20-100 pixels adjacent to the line. The number of pixels was chosen such that the polyline width was as close as possible to the width of the PSM itself, without including any tissue outside the PSM.

Cell counting

Cell counting was performed using a method derived from a standard spot counting protocol by Robert Haase, using the pyclesperanto library (Haase et al., 2020). The DAPI (nuclear) channel was first extracted from the image, and rescaled to have voxels of size 0.5 μm^3. A gaussian blur was then performed on the nuclear channel, with a radius of 0.5 µm (one voxel) in the X and Y dimensions, and zero voxels in the Z dimension. The local maxima was detected, using a 'box' (cubed) connectivity, and radius of 1.5 µm (three voxels) in all dimensions. To merge nearby spots, a binary dilation was performed with radius 1.5 µm

(three voxels) in the X and Y dimensions and 0.5 µm (one voxel) in the Z dimensions, before spots were labelled, the relevant tissue extracted, and the number of unique labels (e.g. number of cells) in the tissue was counted.

The quality of spot detection was verified blind after segmentation, and embryos where spot detection was not accurate were discarded.

DATA AVAILABILITY

Data Availability The quantitative data supporting the findings of this study have been deposited in the Zenodo repository https://doi.org/10.5281/zenodo.23531187. The raw microscopy images generated during the current study are available from the corresponding author upon reasonable request.

Code Availability All custom analysis code and software scripts used for data quantification have been deposited in the Zenodo repository https://doi.org/10.5281/zenodo.23531187 and are publicly accessible at https://github.com/Shannon-E-Taylor/EvolvingInitialConditions.

ACKNOWLEDGMENTS

We are very grateful to Christine Soper, Allex Turner, and Helen Saunders for excellent fish care, and to members of the Verd lab for insightful comments during the research process. The authors gratefully acknowledge the use of the University of Oxford Advanced Research Computing (ARC) facility (http://dx.doi. org/10.5281/zenodo.22558), and the Micron Advanced Bioimaging Facility (supported by Wellcome Strategic Awards 091911/B/10/Z and 107457/Z/15/Z) for their support and assistance in this work. SET was supported by a Clarendon Scholarship, the William Georgetti Scholarship, and a Raymond-Sisam Graduate Scholarship from St Hildas College. JH was supported by a Natural Environment Research Council DTP studentship (grant NE/S007474/1). BV was supported by the John Fell Fund, University of Oxford (0009780), the Royal Society (RGS111324) and the European Research Council (101163722 StG Counts).

AUTHOR CONTRIBUTIONS

Conceptualization: BV. Methodology: SET, JH, BV. Investigation: SET, JH. Visualization: SET. Writing: SET, JH, BV. Editing: SET, JH, BV. Funding Acquisition: SET, JH, BV. Supervision: BV.

AUTHOR COMPETING INTERESTS

No competing interests.

REFERENCES

Abe, G. et al. (2014). "The Origin of the Bifurcated Axial Skeletal System in the Twin-Tail Goldfish". *Nature Communications* 5.1, p. 3360. DOI: 10.1038/ncomms4360.

Aulehla, A. and O. Pourquié (2010). "Signaling Gradients during Paraxial Mesoderm Development". *Cold Spring Harbor Perspectives in Biology* 2.2, a000869. DOI: 10.1101/cshperspect.a000869. PMID: 20182616.

Baer, K. E. von (1828). *Über Entwickelungsgeschichte Der Thiere*. Königsberg: Bei den Gebrüdern Bornträger. DOI: 10.5962/bhl.title.6303.

Ban, H. et al. (2019). "Transcriptional Autoregulation of Zebrafish *Tbx6* Is Required for Somite Segmentation". *Development* 146.18, dev177063. DOI: 10.1242/dev.177063.

Bénazéraf, B. (2019). "Dynamics and Mechanisms of Posterior Axis Elongation in the Vertebrate Embryo". *Cellular and Molecular Life Sciences* 76.1, pp. 89–98. DOI: 10.1007/s00018-018-2927-4.

Bénazéraf, B. et al. (2010). "A Random Cell Motility Gradient Downstream of FGF Controls Elongation of an Amniote Embryo". *Nature* 466.7303, pp. 248–252. DOI: 10.1038/nature09151. PMID: 20613841.

Bhullar, B.-A. S. et al. (2012). “Birds Have Paedomorphic Dinosaur Skulls”. *Nature* 487.7406, pp. 223–226. DOI: 10.1038/nature11146.

Blanchard, G. B. et al. (2009). “Tissue tectonics: morphogenetic strain rates, cell shape change and intercalation”. *Nature Methods* 6.6, pp. 458–464. DOI: 10.1038/nmeth.1327.

Bucklow, C. V. et al. (2025a). “African Cichlid Lake Radiations Recapitulate Riverine Axial Morphologies Through Repeated Exploration of Morphospace”. DOI: 10.1101/2025.05.13.653847.

Bucklow, C. V. et al. (2025b). “Somitic Change Drives Changes in Vertebral Regionalisation in African Cichlids Despite Strong Canalisation of Somite Number”. DOI: 10.1101/2025.05.23.655800.

Burel, J.-M. et al. (2015). “Publishing and Sharing Multi-Dimensional Image Data with OMERO”. *Mammalian Genome* 26.9, pp. 441–447. DOI: 10.1007/s00335-015-9587-6.

Busby, L. and B. Steventon (2021). “Tissue Tectonics and the Multi-Scale Regulation of Developmental Timing”. *Interface Focus* 11.3, p. 20200057. DOI: 10.1098/rsfs.2020.0057.

Choi, H. M. T. et al. (2016). “Mapping a Multiplexed Zoo of mRNA Expression”. *Development* 143.19, pp. 3632–3637. DOI: 10.1242/dev.140137.

Choi, H. M. T. et al. (2018). “Third-Generation in Situ Hybridization Chain Reaction: Multiplexed, Quantitative, Sensitive, Versatile, Robust”. *Development* 145.12, dev165753. DOI: 10.1242/dev.165753.

Chuai, M. et al. (2023). “Reconstruction of Distinct Vertebrate Gastrulation Modes via Modulation of Key Cell Behaviors in the Chick Embryo”. *Science Advances* 9.1, eabn5429. DOI: 10.1126/sciadv.abn5429.

Clark, E. and A. D. Peel (2018). “Evidence for the Temporal Regulation of Insect Segmentation by a Conserved Sequence of Transcription Factors”. *Development* 145.10, dev155580, dev.155580. DOI: 10.1242/dev.155580. PMID: 29724758.

Clark, E., A. D. Peel, and M. Akam (2019). “Arthropod Segmentation”. *Development* 146.18, dev170480. DOI: 10.1242/dev.170480. PMID: 31554626.

Cohn, M. J. and C. Tickle (1999). “Developmental Basis of Limblessness and Axial Patterning in Snakes”. *Nature* 399.6735, pp. 474–479. DOI: 10.1038/20944.

Cooke, J. and E. C. Zeeman (1976). “A Clock and Wavefront Model for Control of the Number of Repeated Structures during Animal Morphogenesis”. *Journal of Theoretical Biology* 58.2, pp. 455–476. DOI: 10.1016/s0022-5193(76)80131-2. PMID: 940335.

Crombach, A. et al. (2016). “Gap Gene Regulatory Dynamics Evolve along a Genotype Network”. *Molecular Biology and Evolution* 33.5, pp. 1293–1307. DOI: 10.1093/molbev/msw013.

Darwin, C. (1859). *On the Origin of Species by Means of Natural Selection*. London: Murray.

Duboule, D. (1994). “Temporal Colinearity and the Phylotypic Progression: A Basis for the Stability of a Vertebrate Bauplan and the Evolution of Morphologies through Heterochrony”. *Development* (Supplement), pp. 135–142. DOI: 10.1242/dev.1994.Supplement.135.

Etoc, F. et al. (2016). “A Balance between Secreted Inhibitors and Edge Sensing Controls Gastruloid Self-Organization”. *Developmental Cell* 39.3, pp. 302–315. DOI: 10.1016/j.devcel.2016.09.016.

Florio, M. and W. B. Huttner (2014). “Neural Progenitors, Neurogenesis and the Evolution of the Neocortex”. *Development* 141.11, pp. 2182–2194. DOI: 10.1242/dev.090571.

Fujimura, K. and N. Okada (2007). “Development of the Embryo, Larva and Early Juvenile of Nile Tilapia *Oreochromis Niloticus* (Pisces: Cichlidae). Developmental Staging System”. *Development, Growth & Differentiation* 49.4, pp. 301–324. DOI: 10.1111/j.1440-169X.2007.00926.x.

Fulton, T., B. Verd, and B. Steventon (2022a). “The Unappreciated Generative Role of Cell Movements in Pattern Formation”. *Royal Society Open Science* 9.4, p. 211293. DOI: 10.1098/rsos.211293.

Fulton, T. et al. (2022b). “Cell Rearrangement Generates Pattern Emergence as a Function of Temporal Morphogen Exposure”. *bioRxiv*, p. 2021.02.05.429898. DOI: 10.1101/2021.02.05.429898.

Galis, F. et al. (2014). “Fast running restricts evolutionary change of the vertebral column in mammals”. *Proceedings of the National Academy of Sciences* 111.31, pp. 11401–11406. DOI: 10.1073/pnas.1401392111.

Giandomenico, S. L. and M. A. Lancaster (2017). “Probing Human Brain Evolution and Development in Organoids”. *Current Opinion in Cell Biology* 44, pp. 36–43. DOI: 10.1016/j.ceb.2017.01.001. PMID: 28157638.

Gomez, C. et al. (2008). “Control of Segment Number in Vertebrate Embryos”. *Nature* 454.7202 (7202), pp. 335–339. DOI: 10.1038/nature07020.

Haase, R. et al. (2020). “CLIJ: GPU-accelerated Image Processing for Everyone”. *Nature Methods* 17.1 (1), pp. 5–6. DOI: 10.1038/s41592-019-0650-1.

Hammond, J. E., C. V. Bucklow, and B. Verd (2025). “Evolvability in Vertebrate Segmentation”. *Seminars in Cell & Developmental Biology* 174, p. 103630. DOI: 10.1016/j.semcdb.2025.103630. PMID: 40768858.

Harima, Y. et al. (2013). “Accelerating the Tempo of the Segmentation Clock by Reducing the Number of Introns in the *Hes7* Gene”. *Cell Reports* 3.1, pp. 1–7. DOI: 10.1016/j.celrep.2012.11.012.

Heemskerk, I. et al. (2019). “Rapid Changes in Morphogen Concentration Control Self-Organized Patterning in Human Embryonic Stem Cells”. *eLife* 8. Ed. by R. Nusse et al., e40526. DOI: 10.7554/eLife.40526.

Holley, S. A. (2007). “The Genetics and Embryology of Zebrafish Metamerism”. *Developmental Dynamics* 236.6, pp. 1422–1449. DOI: 10.1002/dvdy.21162.

Hu, Y. et al. (2018). “A Morphological Novelty Evolved by Co-Option of a Reduced Gene Regulatory Network and Gene Recruitment in a Beetle”. *Proceedings of the Royal Society B: Biological Sciences* 285.1885, p. 20181373. DOI: 10.1098/rspb.2018.1373.

Irie, N. and S. Kuratani (2011). “Comparative Transcriptome Analysis Reveals Vertebrate Phylotypic Period during Organogenesis”. *Nature Communications* 2.1, p. 248. DOI: 10.1038/ncomms1248.

Jaeger, J. and N. Monk (2014). “Bioattractors: Dynamical Systems Theory and the Evolution of Regulatory Processes”. *The Journal of Physiology* 592.11, pp. 2267–2281. DOI: 10.1113/jphysiol.2014.272385.

Kadiyala, U. et al. (2025). “From Genes to Patterns: Five Key Dynamical Systems Concepts to Decode Developmental Regulatory Mechanisms”. *Development* 152.14, dev204617. DOI: 10.1242/dev.204617.

Kawakami, T. et al. (2017). “Prolongation of Somitogenesis in Two Anguilliform Species, the Japanese Eel Anguilla Japonica and Pike Eel Muraenesox Cinereus, with Refined Descriptions of Their Early Development”. *Journal of Fish Biology* 90.4, pp. 1533–1547. DOI: 10.1111/jfb.13249.

Kingsley, E. P. et al. (2024). “Adaptive Tail-Length Evolution in Deer Mice Is Associated with Differential Hoxd13 Expression in Early Development”. *Nature Ecology & Evolution* 8.4, pp. 791–805. DOI: 10.1038/s41559-024-02346-3.

Krol, A. J. et al. (2011). “Evolutionary Plasticity of Segmentation Clock Networks”. *Development* 138.13, pp. 2783–2792. DOI: 10.1242/dev.063834.

Lawton, A. K. et al. (2013). “Regulated Tissue Fluidity Steers Zebrafish Body Elongation”. *Development* 140.3, pp. 573–582. DOI: 10.1242/dev.090381.

Lázaro, J. et al. (2023). “A Stem Cell Zoo Uncovers Intracellular Scaling of Developmental Tempo across Mammals”. *Cell Stem Cell* 30.7, pp. 938–949. DOI: 10.1016/j.stem.2023.05.014. PMID: 37343565.

Li, I.-J. et al. (2019). “Embryonic and Postembryonic Development of the Ornamental Twin-Tail Goldfish”. *Developmental Dynamics* 248.4, pp. 251–283. DOI: 10.1002/dvdy.15.

Maia-Fernandes, A. C. et al. (2024). “Spatio-Temporal Dynamics of Early Somite Segmentation in the Chicken Embryo”. *PloS One* 19.4, e0297853. DOI: 10.1371/journal.pone.0297853. PMID: 38635504.

Malinsky, M. et al. (2018). “Whole-Genome Sequences of Malawi Cichlids Reveal Multiple Radiations Interconnected by Gene Flow”. *Nature Ecology & Evolution* 2.12 (12), pp. 1940–1955. DOI: 10.1038/s41559-018-0717-x.

Mallarino, R. et al. (2012). “Closely Related Bird Species Demonstrate Flexibility between Beak Morphology and Underlying Developmental Programs”. *Proceedings of the National Academy of Sciences* 109.40, pp. 16222–16227. DOI: 10.1073/pnas.1206205109.

Manning, A. J. and D. Kimelman (2015). “Tbx16 and Msgn1 Are Required to Establish Directional Cell Migration of Zebrafish Mesodermal Progenitors”. *Developmental Biology* 406.2, pp. 172–185. DOI: 10.1016/j.ydbio.2015.09.001.

Marconi, A. et al. (2023). “Morphological and Temporal Variation in Early Embryogenesis Contributes to Species Divergence in Malawi Cichlid Fishes”. *Evolution & Development* 25.2, pp. 170–193. DOI: 10.1111/ede.12429.

Marconi, A. et al. (2024). “Genetic and Developmental Divergence in the Neural Crest Program between Cichlid Fish Species”. *Molecular Biology and Evolution* 41.11, msae217. DOI: 10.1093/molbev/msae217.

Martin, B. L. and D. Kimelman (2008). "Regulation of Canonical Wnt Signaling by Brachyury Is Essential for Posterior Mesoderm Formation". *Developmental Cell* 15.1, pp. 121–133. DOI: 10.1016/j.devcel.2008.04.013. PMID: 18606146.

– (2010). "Brachyury Establishes the Embryonic Mesodermal Progenitor Niche". *Genes & Development* 24, pp. 2778–2783. DOI: 10.1101/gad.1962910. PMID: 21159819.

Matsuda, M. et al. (2020). "Species-Specific Segmentation Clock Periods Are Due to Differential Biochemical Reaction Speeds". *Science* 369.6510, pp. 1450–1455. DOI: 10.1126/science.aba7668.

McDaniel, C. et al. (2024). "Spatiotemporal Control of Pattern Formation during Somitogenesis". *Science Advances* 10.4, eadk8937. DOI: 10.1126/sciadv.adk8937.

Mongera, A. et al. (2018). "A Fluid-to-Solid Jamming Transition Underlies Vertebrate Body Axis Elongation". *Nature* 561.7723 (7723), pp. 401–405. DOI: 10.1038/s41586-018-0479-2.

Mora-Bermúdez, F. et al. (2016). "Differences and Similarities between Human and Chimpanzee Neural Progenitors during Cerebral Cortex Development". *eLife* 5. Ed. by A. Musacchio, e18683. DOI: 10.7554/eLife.18683.

Morris, Z. S. et al. (2019). "Heterochronic Shifts and Conserved Embryonic Shape Underlie Crocodylian Craniofacial Disparity and Convergence". *Proceedings of the Royal Society B: Biological Sciences* 286.1897, p. 20182389. DOI: 10.1098/rspb.2018.2389.

Münster, S. et al. (2019). "Attachment of the Blastoderm to the Vitelline Envelope Affects Gastrulation of Insects". *Nature* 568.7752, pp. 395–399. DOI: 10.1038/s41586-019-1044-3.

Murugesan, S. N. et al. (2022). "Butterfly Eyespots Evolved via Cooption of an Ancestral Gene-Regulatory Network That Also Patterns Antennae, Legs, and Wings". *Proceedings of the National Academy of Sciences* 119.8, e2108661119. DOI: 10.1073/pnas.2108661119.

Nikaido, M. et al. (2002). "*Tbx24*, Encoding a T-box Protein, Is Mutated in the Zebrafish Somite-Segmentation Mutant *Fused Somites*". *Nature Genetics* 31.2, pp. 195–199. DOI: 10.1038/ng899.

Niwa, Y. et al. (2011). "Different Types of Oscillations in Notch and Fgf Signaling Regulate the Spatiotemporal Periodicity of Somitogenesis". *Genes & Development* 25.11, pp. 1115–1120. DOI: 10.1101/gad.2035311. PMID: 21632822.

Oates, A. C., L. G. Morelli, and S. Ares (2012). "Patterning Embryos with Oscillations: Structure, Function and Dynamics of the Vertebrate Segmentation Clock". *Development* 139.4, pp. 625–639. DOI: 10.1242/dev.063735. PMID: 22274695.

Osborn, D. P. S. et al. (2020). "Fgf-Driven Tbx Protein Activities Directly Induce Myf5 and Myod to Initiate Zebrafish Myogenesis". *Development* 147.8, dev184689. DOI: 10.1242/dev.184689.

Petridou, N. I. et al. (2021). "Rigidity Percolation Uncovers a Structural Basis for Embryonic Tissue Phase Transitions". *Cell* 184.7, 1914–1928.e19. DOI: 10.1016/j.cell.2021.02.017. PMID: 33730596.

Pinson, A. and W. B. Huttner (2021). "Neocortex Expansion in Development and Evolution-from Genes to Progenitor Cell Biology". *Current Opinion in Cell Biology* 73, pp. 9–18. DOI: 10.1016/j.ceb.2021.04.008. PMID: 34098196.

Raff, R. A. (1996). *The Shape of Life: Genes, Development, and the Evolution of Animal Form*. Chicago, IL: University of Chicago Press. 544 pp.

Rayon, T. et al. (2020). "Species-Specific Pace of Development Is Associated with Differences in Protein Stability". *Science* 369.6510, eaba7667. DOI: 10.1126/science.aba7667.

Romanos, M. et al. (2024). "Differential Proliferation Regulates Multi-Tissue Morphogenesis during Embryonic Axial Extension: Integrating Viscous Modeling and Experimental Approaches". *Development* 151.13, dev202836. DOI: 10.1242/dev.202836.

Rombouts, J., J. Elliott, and A. Erzberger (2023). "Forceful Patterning: Theoretical Principles of Mechanochemical Pattern Formation". *EMBO Reports* 24.12, EMBR202357739. DOI: 10.15252/embr.202357739.

Sáez, M., J. Briscoe, and D. Rand (2022). "Dynamical Landscapes of Cell Fate Decisions". *Interface Focus* 12. DOI: 10.1098/rsfs.2022.0002.

Santos, M. E., J. F. Lopes, and C. F. Kratochwil (2023). "East African Cichlid Fishes". *EvoDevo* 14.1, p. 1. DOI: 10.1186/s13227-022-00205-5.

Schindelin, J. et al. (2012). “Fiji: An Open-Source Platform for Biological-Image Analysis”. *Nature Methods* 9.7 (7), pp. 676–682. DOI: 10.1038/nmeth.2019.

Schröter, C. et al. (2008). “Dynamics of Zebrafish Somitogenesis”. *Developmental Dynamics* 237.3, pp. 545–553. DOI: 10.1002/dvdy.21458.

Schröter, C. et al. (2012). “Topology and Dynamics of the Zebrafish Segmentation Clock Core Circuit”. *PLoS biology* 10.7, e1001364. DOI: 10.1371/journal.pbio.1001364. PMID: 22911291.

Schulte-Merker, S. et al. (1992). “The Protein Product of the Zebrafish Homologue of the Mouse T Gene Is Expressed in Nuclei of the Germ Ring and the Notochord of the Early Embryo”. *Development* 116.4, pp. 1021–1032. DOI: 10.1242/dev.116.4.1021.

Schulte-Merker, S. et al. (1994). “No Tail (Ntl) Is the Zebrafish Homologue of the Mouse T (Brachyury) Gene”. *Development* 120.4, pp. 1009–1015. DOI: 10.1242/dev.120.4.1009.

Seleit, A. et al. (2026). *Heterochrony of Axis Segmentation Underlies Extreme Morphogenesis in the Japanese Eel*. DOI: 10.64898/2026.04.29.721344. URL: https://www.biorxiv.org/content/10.64898/2026.04.29.721344v1 (visited on 09/04/2026). Pre-published.

Serrano Nájera, G. and C. J. Weijer (2023). “The Evolution of Gastrulation Morphologies”. *Development* 150.7, dev200885. DOI: 10.1242/dev.200885.

Serrano Nájera, G. et al. (2025). “Control of Tissue Flows and Embryo Geometry in Avian Gastrulation”. *Nature Communications* 16.1, p. 5174. DOI: 10.1038/s41467-025-60249-8.

Simsek, M. F. and E. M. Özbudak (2018). “Spatial Fold Change of FGF Signaling Encodes Positional Information for Segmental Determination in Zebrafish”. *Cell Reports* 24.1, 66–78.e8. DOI: 10.1016/j.celrep.2018.06.023.

Simsek, M. F. et al. (2023). “Periodic Inhibition of ERK Activity Drives Sequential Somite Segmentation”. *Nature* 613.7942, pp. 153–159. DOI: 10.1038/s41586-022-05527-x. PMID: 36517597.

Steventon, B. et al. (2016). “Species-Specific Contribution of Volumetric Growth and Tissue Convergence to Posterior Body Elongation in Vertebrates”. *Development* 143.10, pp. 1732–1741. DOI: 10.1242/dev.126375.

Stickney, H. L., M. J. Barresi, and S. H. Devoto (2000). “Somite Development in Zebrafish”. *Developmental Dynamics* 219.3, pp. 287–303. DOI: 10.1002/1097-0177(2000)9999:9999<::AID-DVDY1065>3.0.CO;2-A.

Taylor, S. E. and P. K. Dearden (2022). “The *Nasonia* Pair-Rule Gene Regulatory Network Retains Its Function over 300 Million Years of Evolution”. *Development* 149.5, dev199632. DOI: 10.1242/dev.199632.

Thomson, L., L. Muresan, and B. Steventon (2021). “The Zebrafish Presomitic Mesoderm Elongates through Compaction-Extension”. *Cells & Development*. Quantitative Cell and Developmental Biology 168, p. 203748. DOI: 10.1016/j.cdev.2021.203748.

Torres-Paz, J., J. Leclercq, and S. Rétaux (2019). “Maternally Regulated Gastrulation as a Source of Variation Contributing to Cavefish Forebrain Evolution”. *eLife* 8, e50160. DOI: 10.7554/eLife.50160.

Turner, G. F. (2007). “Adaptive Radiation of Cichlid Fish”. *Current Biology* 17.19, R827–R831. DOI: 10.1016/j.cub.2007.07.026. PMID: 17925206.

Vaid, S. and W. B. Huttner (2022). “Progenitor-Based Cell Biological Aspects of Neocortex Development and Evolution”. *Frontiers in Cell and Developmental Biology* 10. DOI: 10.3389/fcell.2022.892922.

Verd, B., A. Crombach, and J. Jaeger (2014). “Classification of Transient Behaviours in a Time-Dependent Toggle Switch Model”. *BMC Systems Biology* 8.1, p. 43. DOI: 10.1186/1752-0509-8-43.

Warmflash, A. et al. (2014). “A Method to Recapitulate Early Embryonic Spatial Patterning in Human Embryonic Stem Cells”. *Nature Methods* 11.8, pp. 847–854. DOI: 10.1038/nmeth.3016.

Weinberg, E. S. et al. (1996). “Developmental Regulation of Zebrafish MyoD in Wild-Type, No Tail and Spadetail Embryos”. *Development* 122.1, pp. 271–280. DOI: 10.1242/dev.122.1.271.

SUPPLEMENTARY MATERIAL

Table S1: Statistics on PSM metrics. Each response variable has been tested for its relationship with somite count and species using linear regression. R^2, slopes, standard errors, F- and P-values, and model fit statistics are reported; $P < 0.005$ was considered significant, using Bonferroni correction for ten statistical tests (green highlights). Blue highlights indicate the lowest residual sum of squares (RSS).

	variable stage					comparison		variable stage + species						
	R^2	slope	95 CI	F statistic	p-value	RSS model 1	RSS model 2	R^2	slope	95 CI	species difference	95 CI species diff.	p count	p species
PSM length	0.71	-13.02	-14.53 — -11.51	285.85	4.4e-33	570125	394490	0.80	-13.68	-14.95 — -12.4	77.95	56.6 — 99.3	1.1e-39	8.4e-11
Notochord length	0.76	-10.13	-11.17 — -9.1	370.54	6.5e-38	266211	211735	0.81	-10.50	-11.43 — -9.56	43.41	27.77 — 59.05	4.4e-42	3.1e-07
PSM width	0.43	-3.43	-4.15 — -2.72	87.78	7.2e-16	129073	123839	0.45	-3.55	-4.26 — -2.83	13.45	1.49 — 25.42	3.3e-16	0.03
PSM depth	0.12	1.11	0.55 — 1.67	15.12	1.7e-04	78637	77451	0.13	1.06	0.49 — 1.62	6.41	-3.05 — 15.87	1.6e-04	n.s.
MPZ length	0.34	-2.89	-3.63 — -2.15	58.49	6.5e-12	137317	102837	0.50	-3.18	-3.83 — -2.53	34.54	23.63 — 45.44	1.6e-14	8.7e-09
Somite length	0.48	-0.75	-0.89 — -0.61	108.45	2.5e-18	5022	4797	0.51	-0.73	-0.87 — -0.59	-2.78	-5.14 — -0.43	9.5e-19	0.02
Notochord width	0.30	-0.54	-0.69 — -0.39	50.77	9.4e-11	5560	5503	0.31	-0.55	-0.7 — -0.4	1.41	-1.12 — 3.93	9.4e-11	n.s.
length:width	0.16	-0.03	-0.04 — -0.01	21.73	8.4e-06	29	27	0.20	-0.03	-0.04 — -0.02	0.23	0.05 — 0.4	5.6e-06	0.01
length:depth	0.37	-0.35	-0.43 — -0.26	68.39	2.5e-13	1680	1680	0.37	-0.35	-0.43 — -0.26	0.14	-1.25 — 1.54	3.2e-13	n.s.
depth:width	0.23	-0.11	-0.15 — -0.07	33.69	5.7e-08	356	354	0.23	-0.11	-0.15 — -0.07	-0.25	-0.89 — 0.39	6.1e-08	n.s.

Table S2: Probability of interaction between species and somite stage Evidence for a statistical interaction was tested using linear regression; R^2 and p-value for each term are reported.

	R^2	p species	p count	p interaction
PSM length	0.80	1.0e-10	2.3e-39	n.s.
Notochord length	0.81	3.4e-07	1.0e-41	n.s.
MPZ length	0.50	9.9e-09	2.0e-14	n.s.

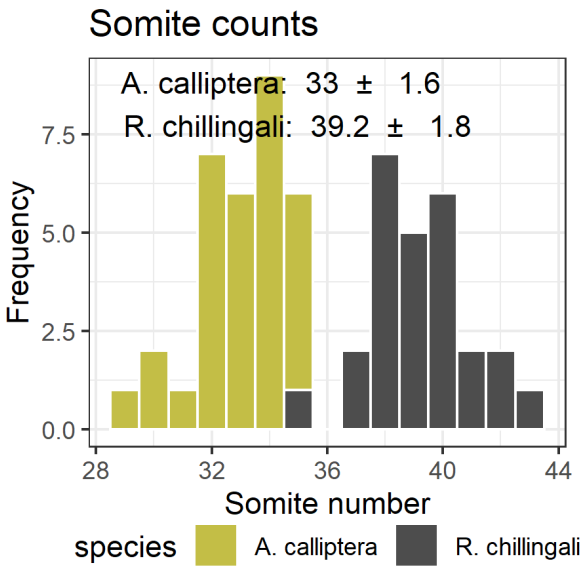


Figure S1: **Number of somites after the end of segmentation in both species.**

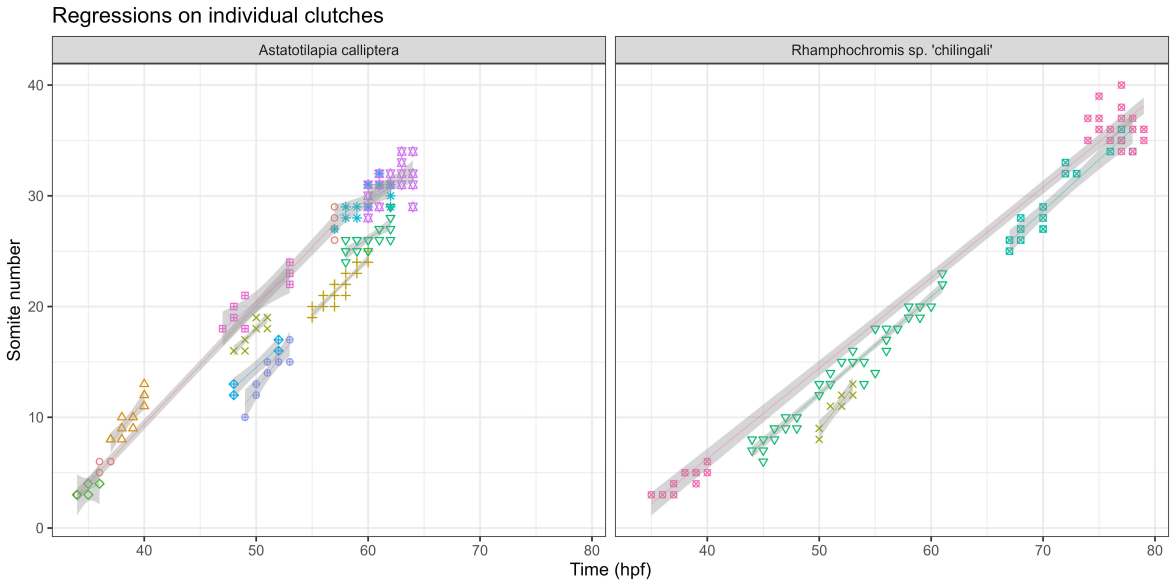


Figure S2: Number of somites versus time in both species. Linear regressions were constructed for both species, for each clutch individually, using ordinary least squares. Colours indicate different clutches. Grey lines indicate the 95% confidence interval.

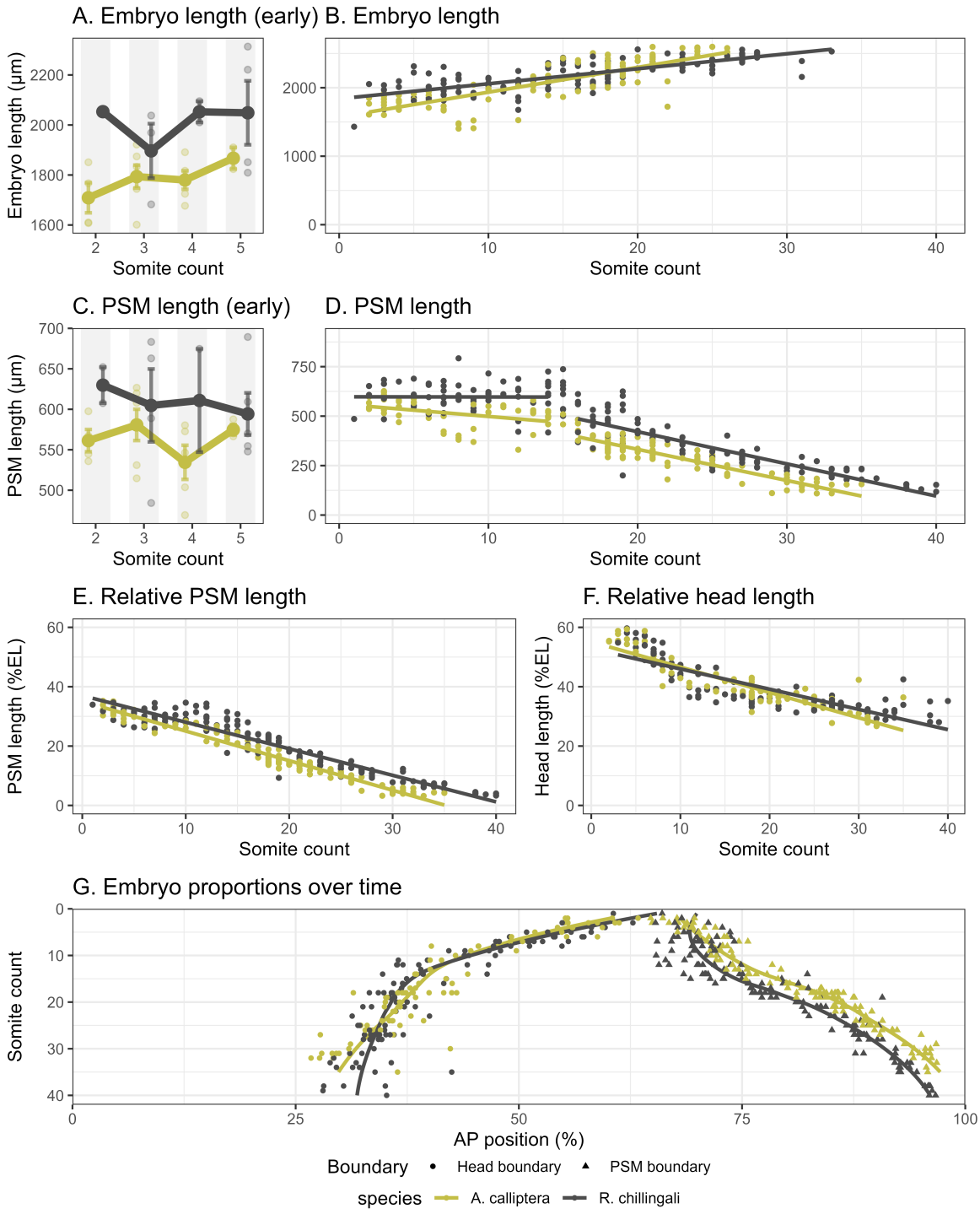


Figure S3: Embryo dimensions differ between species. **A.** Embryo length, in µm, for both species, for embryos between 2 and 5 ss. **B.** Embryo length, in µm, for both species, at different somite stages. **C.** PSM length, in µm, for both species, for embryos between 2 and 5 ss.. **D.** PSM length, in µm, for both species, at different somite stages. **E.** PSM length against somite stage as a percentage of embryo length. **F.** Head length against somite stage as a percentage of embryo length. **G**: Relative head and PSM proportions of embryonic length over time (in somite stage). For **C**, **D**, **E**, **F** the lines represent the linear regression of the variable for each species. For **G**, the coloured lines represent the local regression-based smoothing for each species.

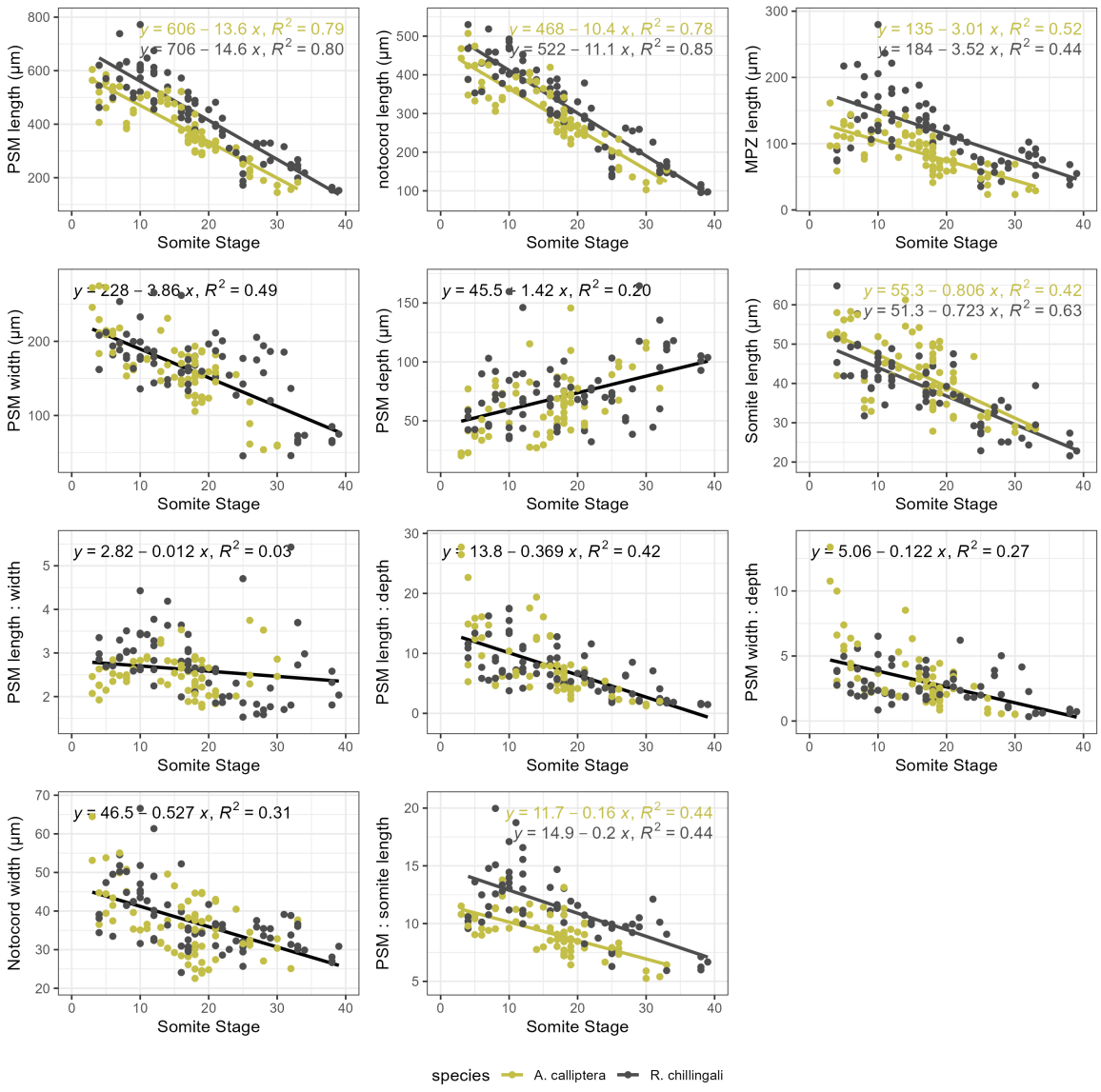


Figure S4: PSM measurements used for PCA. Solid black lines indicate the trendline for measurements where species did not statistically differ, and different coloured lines indicate species-specific trendlines. *A. calliptera*: yellow. *R.* sp. 'chilingali': grey. Somite length: length of the nascent somite. Measurements are as indicated in Figure 3L.

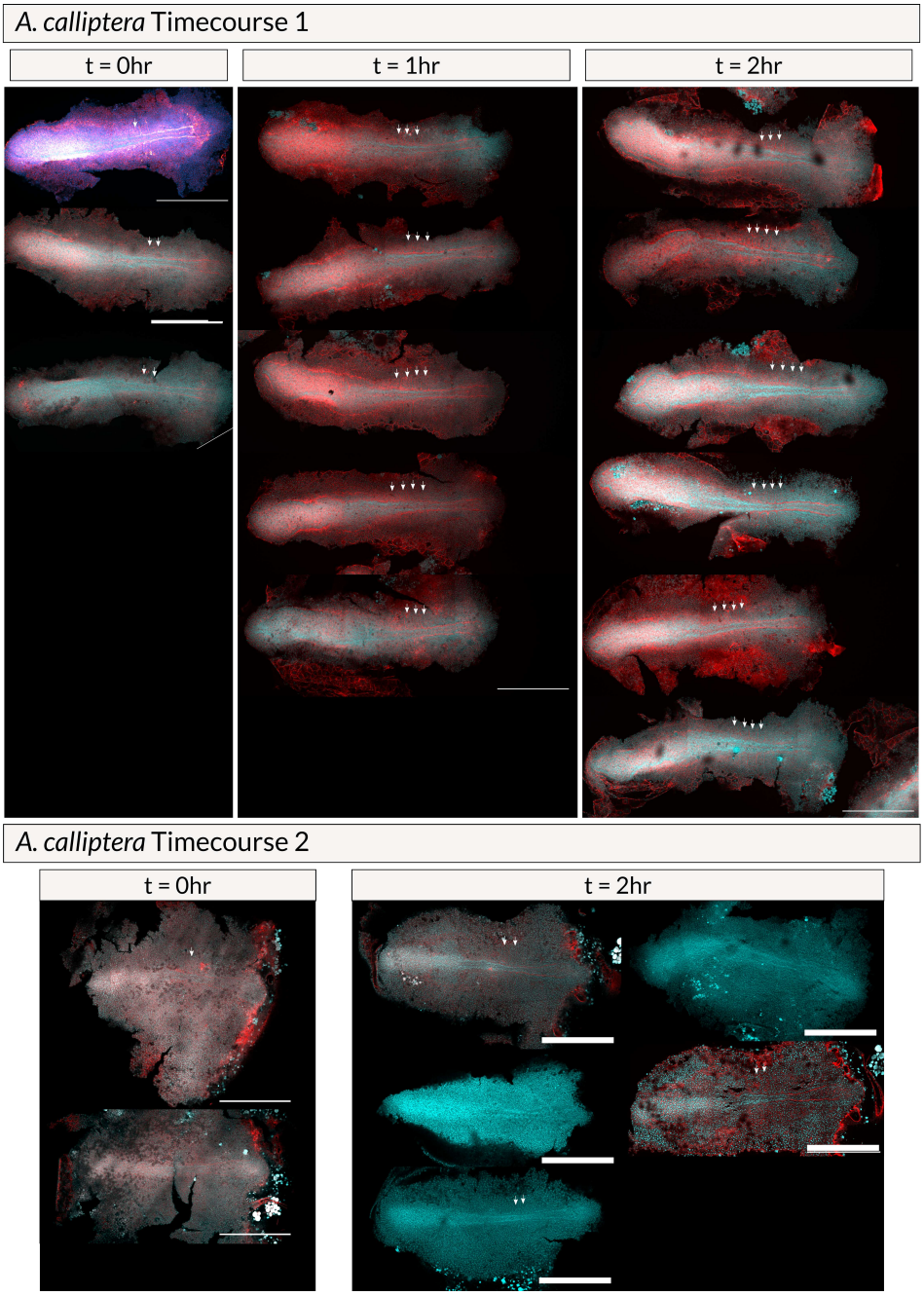


Figure S5: *A. calliptera* somite numbers at the onset of segmentation. Embryos were fixed at hourly intervals, before being dissected and stained with DAPI (cyan) and phalloidin (red). Somites are indicated with arrows. Scale bar: 500 μm. All embryos are oriented anterior left.

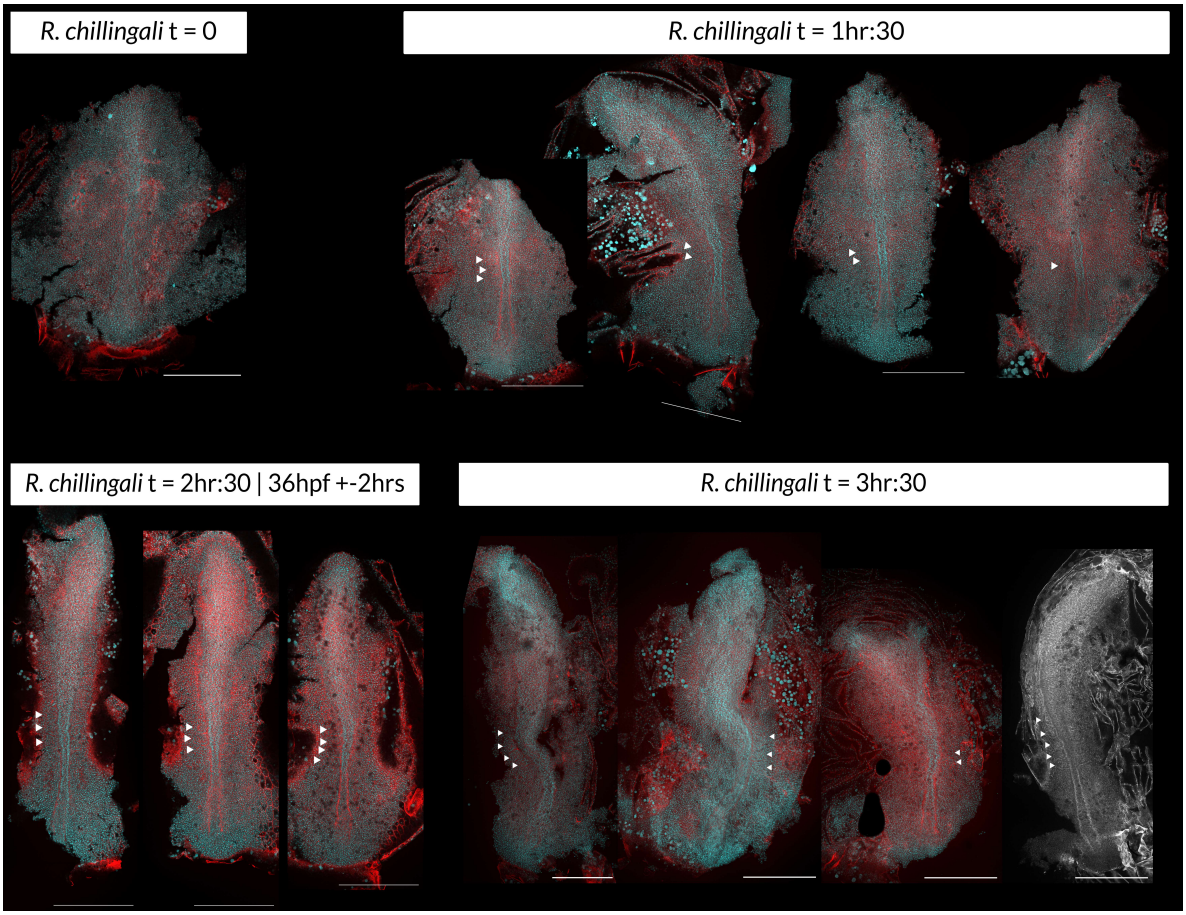


Figure S6: *R.* sp. 'chilingali' somite numbers at the onset of segmentation. Embryos were fixed at hourly intervals, before being dissected and stained with DAPI (cyan) and phalloidin (red). Somites are indicated with arrows. Scale bar: 500 µm. All embryos are oriented anterior towards the top.